Chapter 4

The Intersecting Storage Rings (ISR): The First Hadron Collider

Christian Fabjan and Kurt Hübner

4.1 Introduction

In 1956, with the CERN Proton Synchrotron (CPS) still under construction, a group was formed at CERN to study new accelerators reaching higher energy and/or intensity. This initiative was to assure CERNs future development and strengthen its international standing [1].

The CPS was brought into operation in 1959. It worked very reliably, delivering protons at an energy of 25 GeV. This provided one more reason for the study group to propose adding two *storage rings* tangential to each other and to the CPS. Protons would circulate in opposite directions, stored in the rings for many hours, and would collide at one point providing collisions at a centre-of-mass energy inaccessible with conventional synchrotrons [Box 4.1]. It would require a synchrotron of 1300 GeV to reach the same centre-of-mass energy as these Intersecting Storage Rings (ISR). Clearly, this new technique offered a tremendous leap into new territory for particle physics [2].

By 1962 this idea was taken a step further by proposing concentric rings intersecting at eight points (Fig. 4.1), substantially reducing the foot-print of the facility and allowing a number of experimental groups to work independently and simultaneously.

Remarkably, the approach was driven not so much by the potential users, the particle physicists, but mainly by accelerator physicists and engineers who enthusiastically advocated the new technology. Having had leading positions in the CPS construction team, they brought their experience and expertise to the study group. The particle physicists were occupied with mastering experimentation at the CPS, and the few who reflected on the future rather thought of an extrapolation of the techniques they had been developing there.

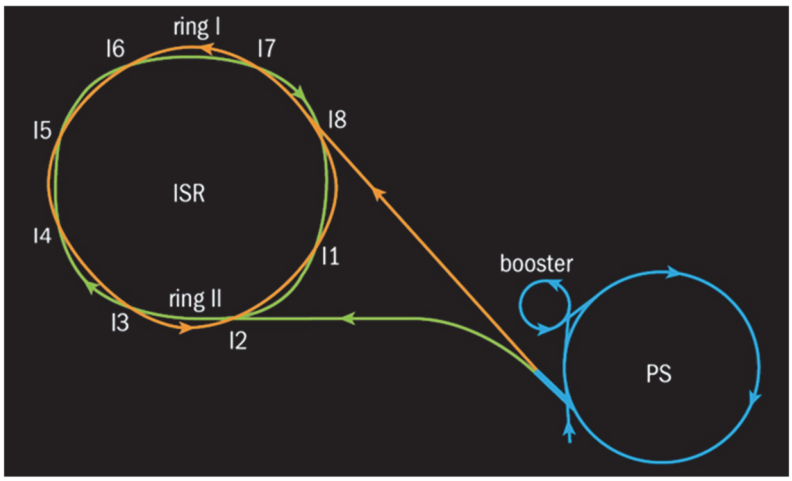

Fig. 4.1. Layout of the Intersecting Storage Rings with the PS injector.

The majority of particle physicists therefore lent support to an alternative to the ISR — a large proton synchrotron of much higher energy than the CPS. This project was preferred as it could provide a large variety of intense secondary beams, and would allow continuing the familiar style of experimentation. Eventually, a proton energy of 300 GeV was agreed upon by these scientists.

After some hesitation and considerable (at times heated) discussions between European particle physicists and CERN management, the latter decided in 1964 to opt for the ISR and to defer the more expensive 300 GeV accelerator.[a] The then Director-General, Victor Weisskopf, showed the vision and persuasiveness to convince both the particle physics community and the CERN Council, which approved the ISR project at the end of 1965 with Kjell Johnsen as project leader. It was an audacious bet to maintain CERN's competitiveness at relatively low cost but at the price of a yet unproven concept. The ISR project is an interesting example how reticent research is driven into a new domain by innovative technology.

The Machine

Already during the design phase two topics were identified as requiring major technological progress: (i) the average residual gas pressure in the vacuum chamber in which the proton beams circulated would have to be less than 10^{-7} Pa

[a]The 300 GeV study was intensively resumed in 1968 and led to the construction of the SPS operating from 1976 onwards (Chapter 5).

(about 10^{-12} times atmospheric pressure) to avoid that the beams would lose protons too quickly or increase their transverse dimensions due to interactions with residual gas. Four orders of magnitude had to be gained relative to vacuum achieved at the CPS. The required Ultra High Vacuum (UHV) technology would have to be developed with European industry. (ii) For the necessarily high interaction rate of the colliding beams, very intense beams had to be accumulated. This was to be obtained by stacking injected proton beam pulses from the CPS by a radio-frequency (RF) system imparting a small, step-wise acceleration to each injected pulse. This technique, first tested in the US, was vital for the new facility and would have to be mastered by CERN. To this end, a 2 MeV electron model of the ISR (CESAR) was constructed and successfully operated in 1964, proving the feasibility of technologies and at the same time qualifying the vacuum industry in a fine example of efficient technology transfer. The success of CESAR provided additional momentum to the project as it progressed through the approval phase.

In January 1971, barely five years after approval and slightly ahead of schedule, beams were injected and stored in both rings, producing the highest energy proton-proton collisions ever achieved on earth. This was duly celebrated at the inauguration ceremony in October (Fig. 4.2).

Fig. 4.2. ISR inauguration: The project leader, K. Johnsen, proudly hands the ISR key to the president of the CERN Council, E. Amaldi. Also on the platform (from left to right): former Director-General W. Weisskopf, the French Secretary of State M. Antonioz, Director-General W. Jentschke and W. Heisenberg, far right.

Colliders **Box 4.1**

Until the 1960s, the interaction of high energy particles with matter was studied in the laboratory by directing beams from accelerators onto targets, in which secondary particles are produced. The energy E_{cm} available in the centre-of-mass system of two colliding particles, one of which is at rest, increases with the square root of the energy E of the incident particle. It was recognized in the 1930s that colliding particles head-on would allow to fully exploit the kinetic energy of both particles, yielding $E_{cm} = 2E$ for identical particles, but it was thought to be too difficult, as the intensity of available beams was low. The principle was however successfully demonstrated in 1961 for e^+e^- collisions in a single storage ring where a bunch of e^+ and one of e^- circulated in opposite directions to meet twice per revolution, to be the first *e^+e^- circular collider*.

A *storage ring* consists of a synchrotron lattice [Box 2.1] and a beam tube under high vacuum to minimize losses and achieve a long beam lifetime. Increasing the number of circulating bunches per ring k_b leads to a proportionally higher collision rate, or luminosity [Box 6.1], as well as an increase in the number of experiments (up to 2 k_b) that can be accommodated. Sufficiently dense and intense beams can be accumulated by repeated injection. The synchrotron radiation emitted by the e^+ and e^- in the bends of the lattice reduces the spread in energy and the amplitude of transverse oscillations, which is important when merging the injected beam with that already stored. But the RF power needed to compensate losses due to synchrotron radiation, proportional to $(E/m_0{\cdot}c^2)^4/\rho$, limits the top energy E of e^+e^- circular colliders, even with a large bending radius ρ, because $e^{+/-}$ mass m_0 is small. For very high energy collisions ($E_{cm} \gtrsim 0.4$ TeV) *linear e^+e^- colliders* are favoured. These consist of opposing linacs with the beams tightly focused at the collision point to get a sufficient rate of interaction.

Proton-proton and $\bar{p}$-p colliders, operate according to the same principle as e^+e^- colliders, with counter-rotating beams. The maximum beam energy is proportional to $\rho{\cdot}B$, where B is the magnetic field, so the design strives for large ρ and B. Two separate rings with opposite vertical magnetic field are required for *p-p colliders*, which provide collisions at intersection points. The magnets can be separate (ISR) or in common, each magnet having two bores (LHC). High beam intensity and/or dense beams are necessary to achieve a useful collision rate (luminosity). The accumulation mechanism of e^+e^- colliders is ineffective as synchrotron radiation is far less for heavy protons than for electrons. Beam intensity is built up quickly, either by injecting pulses side-by-side (ISR) or by sequentially stacking high-density bunches (LHC). This is very demanding for the injector system. If the required energy is higher than the injection energy the beam can be slowly accelerated in the storage ring.

The *p-$\bar{p}$ collider* offers the advantage that counter-rotating beams can circulate in the same vacuum chamber in a single ring, as in e^+e^- colliders, provided the beam is correctly grouped in bunches. The price to pay is that the production of anti-protons requires an elaborate injector chain. A low-density $\bar{p}$-beam is generated by firing a powerful primary p-beam onto a target. This is then accumulated and compressed by many orders of magnitude using stochastic cooling [Box 6.2]. Nevertheless, the number of antiprotons available remains limited, which impacts on p-$\bar{p}$ luminosity.

Unsurprisingly, operation of this totally new machine revealed further technological challenges on the way to reaching, and later exceeding, the design specification, at the pressing request of the experimenters. It was the start of a more than decade-long close and fruitful collaboration between them and the ISR staff [3, 4].

The figure of merit of a particle collider is its luminosity L, which determines the collision rate of the beams [Box 6.1]. It is proportional to the product of the two beam currents divided by the effective height (h_{eff}) in the crossing point. All three parameters change as a function of storage time of the beams and are strongly affected by the quality of the vacuum.

The most pressing issue was the improvement of the UHV system to both increase beam lifetime and reduce the background to the experiments due to lost particles. A vigorous programme was launched to eliminate pressure bumps resulting from the gas release by ions impinging on the vacuum chambers and creating an uncontrolled pressure increase. These ions were created by the ionization of the residual gas traversed by the beam particles and were accelerated by the potential difference between beam and vacuum chamber. These pressure bumps were fought by a series of improvements eventually resulting in a totally upgraded vacuum system: extensive installation of titanium sublimation pumps in addition to the sputter-ion pumps, increase of the bake-out temperature to 300°C and glow-discharge cleaning of the vacuum components. During these upgrade interventions clearing electrodes were also systematically installed to remove the electrons trapped in the beam potential, causing beam instabilities. Ultimately, an average pressure of 4×10^{-10} Pa was reached, a unique achievement in such large a system (two rings of 943 m circumference each) resulting in a useful beam lifetime of up to 50 hours. Even more stringent were the requirements for the vacuum in the interaction regions, where a pressure lower than 10^{-10} Pa was required for acceptable background conditions. At the end of the 1960s it was thought that such a low pressure could only be obtained by condensation cryopumping [Highlight 4.2]. Such low pressures also required the development of vacuum gauges of novel design to measure down to the 10^{-11} Pa range [Highlight 4.3].

Effort was next concentrated on stable operation with high beam currents. This required: (i) using feedback to stabilize the incoming beam; (ii) a very low-noise RF-system for stacking; (iii) control of the electromagnetic forces due to beam current by counteracting them with intensity-dependent adjustment of the magnetic guide field during stacking; and (iv) using other feedback systems to counteract the electromagnetic interaction between the beam and the vacuum chamber.

Continuous improvement of beam diagnostics helped in the quest for ever increasing beam currents which eventually reached routinely 40 A, with a record of 57 A, corresponding to 1.14×10^{15} protons.

The ultimate increase in luminosity was achieved by further decreasing h_{eff} through stronger focusing of the beams at one of the interaction points with a "high luminosity insertion". It was initially implemented with focusing magnets having copper coils and later with more powerful superconducting magnets [Highlight 4.4]. These superconducting magnets, operated at 4.5 K, were installed in cryostats which were fed with liquid helium coolant via novel long screened and flexible coaxial transfer lines. Maximum use was made of the cooling potential of the He vapour from the baths to cool current leads, thermal shields and the lines [Highlight 4.5]. This technological advance was very valuable for superconducting equipment and is now extensively used at the LHC and worldwide.

For the precise determination of luminosity a new technique was invented to accurately measure h_{eff}, the so called "Van der Meer method" [Highlight 4.6], and the relative precision of the beam current measurement was pushed to nearly 10^{-8} with novel current transformers operating at up to 60 A.

During the final years of ISR operation the beam energy was pushed to a maximum of 31.4 GeV, beyond the 26.5 GeV provided by the CPS by the novel acceleration technique of RF phase displacement. It is a tribute to the flexibility of the combined CPS-ISR operation that besides protons the ISR would later store other particles, enabling the study of d–d, p–d, α–α, α–p, and p–antiproton collisions.

However, the single most outstanding ISR legacy to accelerator technology was the development and experimental proof of "Stochastic Beam Cooling", a technique to squeeze the particle beams and hence increase the luminosity. It takes advantage of the so-called Schottky noise, a statistical signal generated by the finite number of randomly distributed particles in a beam. The theory of Stochastic Cooling was initially developed by S. van der Meer in 1968, but appeared technologically too far-fetched. In 1972 with the advent of highly sensitive spectrum analysers it became possible for the first time to observe Schottky noise on the ISR beams. This observation motivated S. van der Meer to publish his concept of "Stochastic cooling" and led to its experimental proof in the ISR. It launched a development of what would later lead to the attribution of a Nobel Prize (Chapter 6 and Box 6.2). The observation of Schottky noise allowed also a revolutionary leap in beam diagnostic technology, resulting in a hitherto unknown means to non-intrusively monitor in real time many parameters of the beam. It has become a standard method of beam monitoring and diagnostics.

The ISR was a unique tool for particle physics which surpassed many design parameters, such as by a factor 35 the design luminosity, due to perseverant

development of leading-edge technologies by a very devoted and stable staff complement. Most importantly, the ISR served as a test bed and laid the foundation for future Nobel-Prize winning CERN facilities, the Proton–Antiproton collider and the LHC.

Experimental Programme

While the very intense development phase for the ISR machine extended over many years, the committee guiding the ISR experimental programme (ISRC) started its work relatively late, just two years before the collider start-up planned for mid-1971. Two major lines of experimental programmes emerged: "survey" experiments to understand known physics in the new energy regime and "discovery" experiments searching for the Unknown.

In proton–proton collisions particles interact predominantly through the strong or hadronic interaction. In the late 1960s hadronic physics was couched in terms of phenomenological descriptions, lacking a deeper, fundamental understanding and providing little — sometimes even erroneous — guidance for experimental research. The elements of today's physics understanding, the Standard Model (SM) [Box 6.4] were just starting to take shape. The incipient revolution that was to establish the SM was paralleled by a revolution in experimentation. In 1968, Georges Charpak (Nobel Prize 1992) and collaborators had demonstrated the concept of a new particle position detector, the Multiwire Proportional Chamber (MWPC) [Highlight 4.8], propelling the community with a stroke of genius into the digital age. Nor should the sociological factor be forgotten: small groups, beam exposures of a few days to a few weeks, quick and easy access to the experimental apparatus, characterized the style of experimentation of the time.

The turmoil provoked by three simultaneous uprisings — the emerging SM confronting limited physics understanding, new tools sweeping away old experimental methods and a collaboration sociology struggling to adapt to new experimental imperatives — put its stamp on the early research programme. Particle physics was at the dawn of a "New Age". Experimentation at the ISR contributed to the "New Enlightenment" [5].

The first years of experimentation, 1971 to 1974

These brought a rich harvest of physics surprises. Among the lasting contributions were the startling observation of the rising of the total-cross section with the centre-of-mass energy, related to the effective size of the proton, and the measurements of elastic scattering, which leaves the protons intact [6]. It required to position particle detectors to within millimetres of the circulating proton beams, a feat accomplished with ingenious technology and excellent collaboration

between the machine and experiment staff [Highlight 4.7]. The most sensational early discovery, however, was the observation of energetic particles frequently produced at very large angles relative to the direction of the proton beams [7]. It revealed also in the strong interactions the point-like constituents of the proton, as previously observed with the electromagnetic probe [8]. It confirmed the internal structure of the proton, containing the whimsically called "quarks". That protons contain quarks was the emerging consensus. Yet all experimental attempts to detect them as free particles failed, a major ISR legacy: "confinement" was recognized to be a fundamental, unique property of the strong interaction, profoundly shaping its understanding.

The Split-Field Magnet (SFM) was the first general-purpose ISR experimental facility. It was proposed in 1969 by Jack Steinberger, Nobel Prize 1988, as the strategy for exploring *terra incognita* at the ISR. Audaciously, it bet its existence on the novel MWPC-detector technology, invented just one year earlier. Within five years the facility was built and instrumented with 50,000 MWPC detector channels — an astronomically large number at the time. The simultaneous revolution in the electronics industry was a godsend: The invention of integrated electronic circuits (ICs) provided a cost-effective way of equipping the detector channels with signal processing electronics. The SFM, however, was conceived with the physics prejudices of the late 1960s: hadronic physics phenomena would reveal themselves in the direction about the incident particle beams, where most of the particles are produced. It was not optimal for the unexpected "real action", the new emerging physics with signatures predominantly at large angles.

While the production of energetic particles at large angles at surprisingly high rates was one of the early ISR physics "sensations", it was an equally unexpected, ferocious background to other new physics phenomena. It prevented ISR experimenters from discovering the J/ψ due to their limited experimental set ups. This particle was observed simultaneously at two American accelerator laboratories in 1974. It implied the existence of a further, fourth quark, the so-called charm quark, a crucial building block of the SM.

1974–1977: Learning the lessons

The discovery of the J/ψ brought sobering soul-searching to the ISR teams and painfully highlighted the lack of an experimental facility optimized for exploration of the new physics landscape [9]. Such a facility would be centred on a new major magnet. Several groups were studying a facility based on a superconducting solenoid, while another team explored a toroidal geometry. A working group, constituted by the ISR Experiments Committee, ISRC, received the remit to motivate and conceptualize a possible new magnetic facility. With exemplary speed — January to March 1976 — the working group documented the physics

case and explored magnets and instrumentation, but even after extending discussions until August shied away from making a recommendation as to the magnet topology. A workshop in the autumn also failed to choose between solenoid and toroid, leaving it to the ISRC to clearly and decisively motivate its preference for a superconducting solenoid with large, openings in the return yoke for detector instrumentation. The merits of the toroidal geometry were recognized but considered too unproven for rapid realization: it would be another 30 years before a major toroidal magnet would be built for proton–proton collider physics — the ATLAS Muon Spectrometer Toroid [Highlight 8.12]. Finally, the CERN management also rejected the ISRC proposal of the large superconducting solenoid as being too costly and taking too long to build.

This working group nevertheless had a profound influence on CERN's research agenda. It provided an assessment of state-of-the-art collider experimentation and technologies. Many members of the group would use their work to shape the UA1 and UA2 facilities [Highlights 6.5 and 6.6] at the Proton–Antiproton collider, which were proposed at about the same time.

At the 1976 autumn workshop an innovative solenoidal magnet had been proposed, the Open Axial Field Magnet [Highlight 4.11]. Following the refusal to support a large superconducting facility this more modest spectrometer magnet was to become the centrepiece for the Axial Field Spectrometer (AFS). The AFS incorporated several state-of-the-art detector technologies. It was the first facility at a hadron collider providing very large solid angle coverage for the momentum and energy measurement of particles. It was designed to operate at collisions rates exceeding one million collisions per second, a totally new regime of experimentation. It required the development of a — for hadron colliders novel — "drift detector" [Highlight 4.8], which could register millions of particles per second and measure their trajectories with bubble-chamber type detail and with an accuracy of 0.1 mm. The energy measurement of all the particles was a further essential, new requirement. The technique is called "Calorimetry" [Highlight 4.10]: the particles are absorbed in specially selected dense materials, in which detectors are embedded which measure the cascade of particles resulting from the absorption process [Box 6.3]. The physics research demanded energy measurements at the percent level, prompting major R&D programmes. One technique used the ionization in liquid argon produced by the particles in the cascade, a concept, which later would be employed in many other experiments. Electrons and muons frequently reveal new physics. For the identification of electrons the effect of "Transition Radiation" [Highlight 4.9] was used for the first time and developed into a practical instrument: Ultra-relativistic particles, e.g. energetic electrons, produce soft X-rays in the passage through "radiators", a few

hundred 20 micron-thin lithium or polyethylene foils, spaced some 200 microns apart. A special form of MWPCs was developed to detect these X-rays, covering many square metres.

These more evolved and novel experimental approaches brought a new level of complexity and longer lead-times from proposal to data-taking: the fruit of these efforts came a few years too late to make the potentially grand impact that was expected from, and deserved by the ISR. Despite this somewhat critical assessment of the experimental situation, a wealth of significant results were obtained, all of which contributed to shaping our understanding, as documented e.g. in [10].

Final years of ISR operation, 1977 to 1983

The experimenters focused on a variety of rare and energetic phenomena: leptons, photons, charmed particles, jets and search for new particles with masses beyond 30 proton masses. This strategy was vindicated by the discovery of the Upsilon (Y) particle, about ten times more massive than the proton, albeit at the U.S. Fermi National Laboratory in 1977. This was a further crucial building block of the SM and yet another cruel blow for the ISR, especially as the first evidence for the Y at the ISR was obtained just five months later by the R806 collaboration [11].

The evolving physics understanding put a stamp on the research programme and consequently on machine operation: go for the highest possible collider energy and collision rates. The collision energy was pushed to 63 GeV, and record-breaking collision rates in excess of one million per second were achieved — a successful rehearsal for the LHC. This operation allowed a multifaceted programme with emphasis on understanding the hadronic interactions through precise tests of the emerging theory, Quantum Chromodynamics, QCD [10] [Box 4.2]. One early major support of QCD was the discovery by the AFS collaboration (Fig. 4.3) of the prompt energetic photon production in p–p collisions, the QCD analogue of the electromagnetic Compton scattering. These photons are predominantly produced in the scatter of a quark on a gluon, providing evidence for the existence of gluons. The observation of "jets", the indirect manifestation of quarks and gluons, concurrent with the observations at the Proton–Antiproton collider, was further strong evidence for QCD [10, 11].

The ISR was a superb machine, a test bed for ground-breaking accelerator and detector technologies. It was a powerful and well-performing collider, but the detectors it would have deserved and required for discoveries within its reach came too late. One reason was that its experimental programme, starting in 1971, was in competition with that of the SPS, approved in the same year, resulting in tight resources, but the fact is that with regard to the experimental programme the physics community was simply not prepared for the enormous jump in energy and physics potential that the ISR provided.

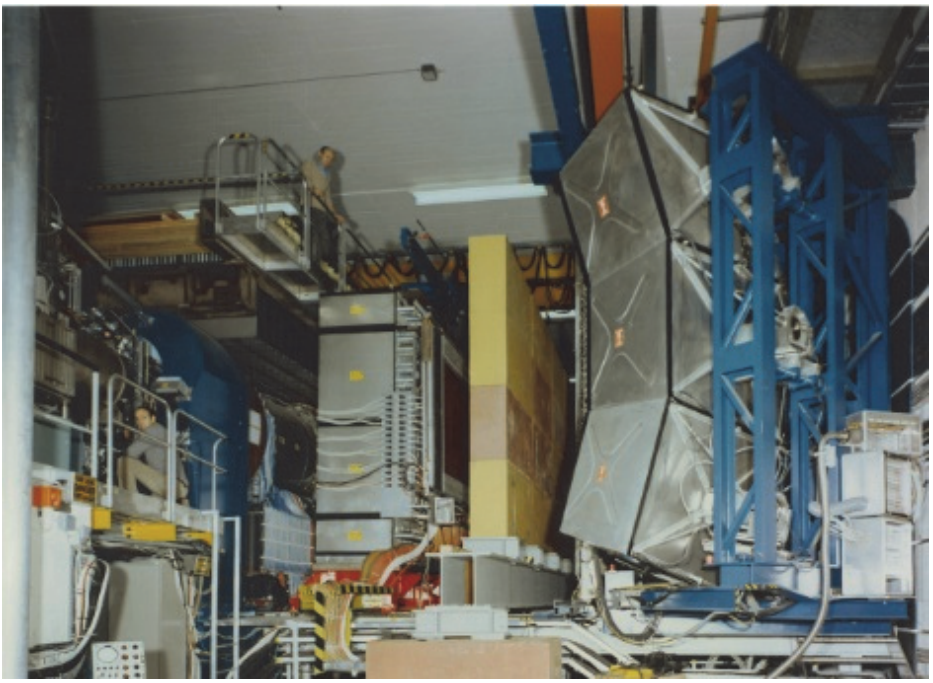

Fig. 4.3. Partial view of Axial Field Spectrometer at I8. The vertical uranium/scintillator hadron calorimeter (just left of centre) is retracted to give access to the cylindrical central drift chamber. The yellow iron structure served as a filter to identify muons, with MWPCs and the array of Cherenkov counters to the right.

By the end of 1983 the CERN Proton-Antiproton collider had produced the first W- and Z- bosons, carriers of the electroweak interaction, a milestone towards the completion of the SM. The construction of LEP had started, which would vindicate the SM with near perfection. For the CERN management it was time to turn a page. At the closure ceremony of the ISR in June 1984, the former Director-General and staunch ISR supporter Viktor Weisskopf said he "had come to praise the ISR…The really important thing about the ISR is its success as an instrument, because *that fact did change the landscape of high energy physics*."

Quantum chromodynamics (QCD) **Box 4.2**

In 1957 electron-proton scattering experiments showed that the proton has a finite size (about 10^{-13} cm radius), and in 1968 that it contains point-like scatterers, later identified as *quarks*. The quark model brought a dramatic simplification, explaining all known hadrons as bound states of these constituents: 3 quarks for baryons, a quark and antiquark for mesons. The spectroscopy of strange, charmed and beauty particles, and the discovery of the top quark established the 3 "families" [Box 6.4].

Colour, a new quantum number proper to quarks, was proposed in 1964 and *QCD*, starting from a model with 8 *gluons* as force carriers and a strong coupling constant α_S, was progressively developed to become the modern theory of the strong interaction. Experimental evidence for the gluon came in 1979. However, there remained a paradox: quarks and gluons appeared to be strictly *confined* within hadrons by a strong force, as if a "spring" prevented them being pulled apart until it broke, producing a jet of hadrons; but when struck by hard photons or W (i.e. lepton or neutrino deep inelastic scattering) quarks inside hadrons appeared to be free and point-like, not interacting with each other, but sharing the hadron momentum, a property responsible for *scaling*, i.e. having collision properties dependent only on dimensionless kinematical parameters, but not on an absolute energy scale.

The strong self-interaction (S-I) of gluons is the key to this mystery. In 1973 it was demonstrated that at high energies, i.e. at short distances between quarks, the colour coupling constant α_S tends to zero, referred to as *asymptotic freedom.* At long distance or low energy, the gluon S-I makes α_S grow, leading to *confinement*. Thus α_S "runs", i.e. changes with the energy scale or resolving power [Box 5.1].

QCD offers another amazing fact. Usually the mass of an object is the sum of masses of its constituents. However, already the atomic nucleus shows a tiny mass defect, which is the key to nuclear energy. For protons and neutrons, the mismatch becomes dramatic: they have a mass of about one GeV/c^2, but are made of "up" and "down" quarks of a few MeV/c^2 and of massless gluons. It is actually the kinetic energy of the frantically moving constituents which is responsible for most of their mass, hence of the mass of the visible universe, a condition referred to as "*mass without mass*".

In the expanding (cooling) universe the confinement of previously free quarks into hadrons, occurred during the "*quark-hadron transition*", a few μs after the Big Bang. Colliding energetic heavy ions allows us to re-create microscopically the temperature conditions reigning at that time. One observes effects interpreted as a brief inverse phase transition with deconfined quarks and gluons: the "*Quark-Gluon Plasma*".

Beyond QCD basic principles, its complex manifestations in multi-particle final states give rise to the main background in the search for new physics beyond the SM. Due to S-I, and large α_S, sorting through this is a monumental task. When LHC protons collide one has to know their composition in terms of elementary objects, i.e. the fractions and kinematic distributions of valence (leading) quarks, gluons and pairs of "sea" quarks and antiquarks of all flavours born from gluon splitting (*scaling violation*).

For further reading: F. Wilczek, QCD Made Simple, *Physics Today*, **53-N8** 22-28, (2000).

4.2 Vacuum Pumping by Freezing Molecules

Cristoforo Benvenuti

For the ISR intersections, where the p–p collisions take place, a pressure lower than 10^{-10} Pa[b] was required to minimize the disturbing proton–gas interactions. This pressure range corresponds to a molecular density of 10^3 to 10^4 molecules per cm^3. At the time of the ISR project proposal, condensation cryopumping was thought to be the only way to achieve this goal. This technique is based on the condensation of the residual gas molecules onto a metal surface having a temperature at which the vapour pressures (VP) are below the desired level.

At the boiling temperature of liquid helium (4.2 K) all condensable gases display VPs lower than 10^{-11} Pa, with the exception of hydrogen, H_2, for which it is higher by many orders of magnitude. However, by extrapolating its VP curve, a sufficiently low H_2 pressure should be within reach at 2 K. In order to verify experimentally the validity of this extrapolation, the equilibrium pressure of condensed H_2 was investigated. The initial results were surprising: below about 3 K this pressure departed from the VP curve, showing an irreducible limitation in the $10^{-7}/10^{-8}$ Pa range, no matter how low the condensation temperature. Further studies showed that this limit is proportional to the room temperature radiation absorbed on the metal surface where condensation occurs [12].

Phonons, the quanta of the atom's energy in a solid, are produced in the metal substrate by the absorbed radiation. It was natural to assume that these phonons could induce molecular desorption when reaching the surface of the condensed H_2. For this to be possible, they should cross the H_2 layer. Hydrogen is very particular in this respect; it is the only solidified gas able to transmit phonons of energy in excess of what is needed to desorb a molecule. A spectacular confirmation of this mechanism was obtained by interposing below the condensed H_2 a thin layer of another gas (e.g. N_2 or Ar) which could inhibit the transmission of the energetic, disturbing phonons. The interposed gas layer produced the expected effect and the H_2 pressure limit was decreased to below 10^{-10} Pa [12].

It would obviously be strange to inject heavy gases in an ultra-high vacuum system to improve the pumping of H_2, but fortunately a more reasonable alternative exists. The disturbing energetic phonons are produced by the thermal radiation from room temperature surfaces, so if the condensing surface is well protected by a low temperature shield, desorption can be decreased. In the CERN design (Fig. 4.4, left), only 5×10^{-4} of the radiation impinging on the shield

[b]The pascal, Pa, one N/m^2, is the official unit of pressure. It replaced the Torr, which is 133 Pa.

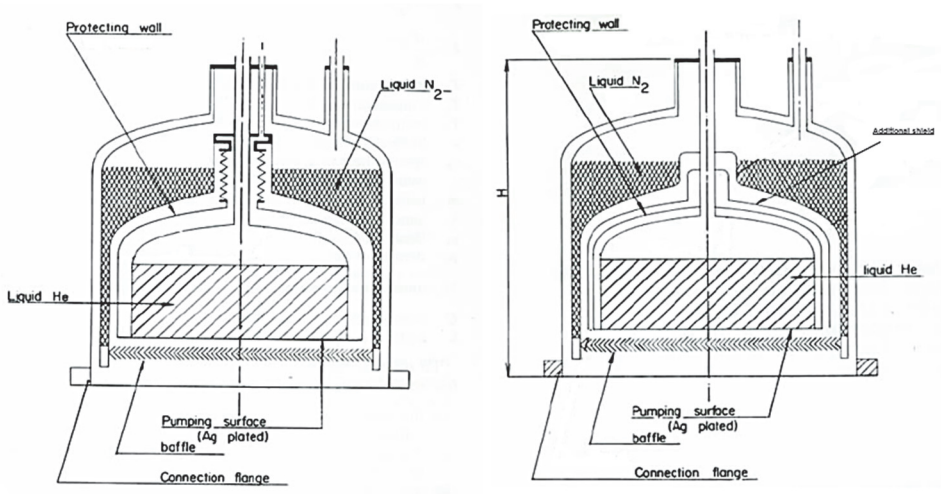

Fig. 4.4. (Left) first model — the function of the protecting wall is to avoid gas release due to the variation of He level. The double wall volume is under vacuum [13]. (Right) improved model — the double wall volume is filled with Ne, which provides good thermal contact during the initial cooling and thermal insulation at 4.2 K [14].

(a baffle cooled with liquid N_2) is transmitted to the condensation surface, resulting in a H_2 radiation induced pressure below 10^{-10} Pa [12]. The improved shield also led to a welcome reduction in the consumption of liquid helium.

One of the ISR experimental areas (point 6) was equipped with two large cryopumps, where a pressure lower than 10^{-10} Pa was achieved.

The initial model [13] was later improved by introducing an additional shield cooled by the evaporating He (Fig. 4.3, right). The liquid He consumption was then so low that it was possible to operate 200 days without refilling the 11 litre vessel [14]. The improved model was later used for the H_2 jet target experiment at ISR point 8, and for the Viksi cyclotron at the Hahn Meitner Institute in Berlin.

Cryopumping provides the advantages of a very high pumping speed and low ultimate pressure. On this ground it was considered the best pumping technique for about 10 years, at the end of the 1970s. But the advent of commercial large turbomolecular pumps and the use of Getter pumping (in the form of either Titanium sublimation or Non Evaporable Getters (NEG)) to produce extremely low pressures reduced the interest for this technique, which suffers the complication of having to provide and handle liquid helium.

Besides being a facility for physics research, the ISR was also a test bench for solutions which could be later adopted for a larger accelerator equipped with superconducting magnets. In these magnets the vacuum chamber would be cold and its behaviour with respect to the ISR pressure instabilities would be different.

To evaluate such "cold bore" behaviour, a cryostat containing a 1.3 m long vacuum chamber cooled at temperatures from 2 K to 200 K was installed in the ISR. Various quantities of different gases were condensed on the chamber surfaces while beams up to 40 A were circulating [15]. The vacuum was found to remain stable even in the most severe conditions thanks to the large pumping speed provided by cryopumping.

These positive results and the solid experience gained provided the confidence to propose cryopumping on a large scale in LHC where it is now used successfully in the cold sectors stretching over about 18 km (Chapter 8).

4.3 How to Measure Almost Nothing

Cristoforo Benvenuti

In the technology of Ultra High Vacuum, pressure is usually measured by means of ionization gauges. In such gauges the electrons emitted by a hot filament (cathode) are accelerated by the positive potential of a grid (anode) and ionise the residual gas molecules, which are then collected by a third electrode, the ion collector. The current reaching the collector is proportional to the pressure. However, at low pressure, the performance of this gauge is limited due to X-rays produced by electrons striking the grid. This radiation extracts electrons from the ion collector resulting in a current (I_x) that falsifies the result.

A major improvement was achieved by Alpert in 1950 who replaced the ion collector surrounding the grid with a thin wire at its centre (Fig. 4.5a). The large reduction of the collector area resulted in a decrease of I_x, and the low pressure limit of the gauge (called the Bayard-Alpert gauge, B.A.) was reduced by a few orders of magnitude, down to the 10^{-9} Pa range. Alpert himself remarked a few years later that it might not be possible to reduce I_x indefinitely by reducing the collector diameter because "there may be a critical size below which the probability of collecting ions reduces as rapidly as does the X-ray effect" [16]. This was because the tangential component of the velocity of the ions inside the grid would prevent a fraction of them from reaching the collector when first approaching it, and — assuming the electric field inside the grid to be perfectly radial — they would never be collected. Decreasing the collector diameter below about 0.1 mm would decrease I_x, but the ion current would also decrease in the same proportion and the performance of the gauge would not improve. This was confirmed by theoretical calculations and some experiments, and became vacuum technology dogma.

But such ideal conditions are always rare. The radial field inside the grid is perturbed both by the potential of the nearby filament and by space charge due to the accumulation of ions, which being fully enclosed by the grid are, in time, bound to be collected. This effect was confirmed by experiment at CERN showing that in fact ion collection efficiency remains constant for collector diameters down to 0.025 mm, extending the low pressure range of the B.A. gauge to 10^{-10} Pa [17].

This study had been motivated by the need to measure pressures much lower than that originally specified for the ISR (10^{-8} Pa), resulting from the vacuum system upgrade referred to in the introduction. Based on this work some 500 B.A. gauges of improved design were produced by industry and installed in the ISR, where they measured pressures typically in the low 10^{-10} Pa range. After the dismantling of the ISR these same gauges were used for LEP and later for LHC, some 40 years after their production.

For the ISR experimental areas, a few gauges were needed to measure pressures lower than 10^{-10} Pa, so a type was required that performed better than the improved B.A. gauge at such low pressures. Outside CERN and due to the above-mentioned dogma, all development of low pressure gauges was based on the same approach of moving the ion collector to outside the grid volume and properly shielding it from the detrimental X-rays. Various commercial gauges were tested, all of the

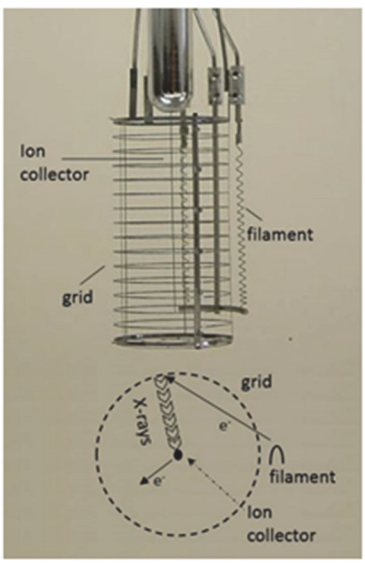

Fig. 4.5a: The Bayard-Alpert gauge, with an illustration of the X-ray effect.

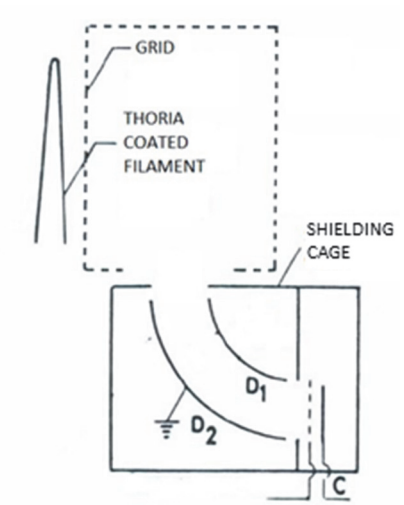

Fig. 4.5b: Schematic view of the Helmer gauge: D_1, D_2 electrostatic deflector, C ion collector [20].

"external collector" type, the most promising model being one that was marketed under the trade name of the Helmer gauge [18], with a power supply adapted for the 10^{-11} Pa range. The design of this gauge is shown in Fig. 4.5b. The ions produced inside the grid are extracted and driven by an electrostatic deflector to the ion collector, which is well shielded from X-rays. A thorough analysis of the gauge performance [19] showed that the atoms sublimating from the electron filament at ~ 2000 °C were producing a local parasitic pressure in the low 10^{-10} Pa range, in spite of the extremely low vapour pressure of tungsten, the material of the filament. By coating the filament with a better electron emitter (thoria) the filament temperature could be reduced to about 1000 °C, low enough to avoid atomic sublimation. By enlarging the grid diameter the length of the path of electrons inside the grid was increased, so extending the access of the gauge to the low 10^{-12} Pa range, which was and still is the lowest pressure ever measured inside a vacuum system [20].

4.4 Superconducting Magnets: Squeezing Beams to Extract More Collisions

Romeo Perin

The two main parameters of a colliding beam machine are the beam energy and luminosity [Box 2.1]. The energy is given by the size of the rings and the magnetic bending field: it cannot be altered, but there are ways of increasing luminosity. At a crossing point of the ISR the luminosity, inversely proportional to the height of the particle beams, can be increased by inserting a local focusing structure consisting of a pair of quadrupole magnets on either side of the interaction region (a quadrupole produces zero field on the axis and a linear gradient of field across the aperture). The concept was first validated with normal magnets, but stronger field gradients would be needed to increase luminosity by the desired factor of at least five. This would require superconducting quadrupoles — but of greater size, strength and quality than had been previously attained [Box 4.3]. In 1973 an R&D effort was initiated to verify the feasibility that culminated in the successful test of a prototype built at CERN [21, 22]. On this basis, specifications were written and orders placed in 1977–8 for critical components and for manufacture of eight quadrupoles. The high luminosity insertions (one per beam) started regular operation in 1981, as the first ever superconducting magnet system in an operating accelerator.

Cross-sectional views of the cryo-magnet are shown in Fig 4.9 [Highlight 4.5]. The main components of the quadrupole are: the room temperature bore, a stainless steel tube supporting 6-pole and 12-pole correction windings (which also

Superconductivity for magnets: A gift of nature **Box 4.3**

Superconductivity is observed in many metals and some ceramics. When such materials are cooled to temperatures ranging from about 100 kelvin (K) (about minus 173 °C), to near absolute zero (0 K), at a given *critical temperature* (T_c, a characteristic of the material) their electrical resistance suddenly vanishes. Besides the critical temperature, superconductors also feature a critical field ($\mu_0 H_c$), i.e. the magnetic field above which the material is not superconducting irrespective of the temperature. Examples of critical temperature and critical field are shown in the table. The current density that can be present in the superconductor thus depends on both the temperature and magnetic field, and for a material to be superconducting it must function beneath a *critical surface* as shown in the figure.

Material	T_c (K)	$\mu_0 H_c$ (T)
Tin-lead (Sn60-Pb40)	7.8	< 2
Niobium (Nb)	9.5	< 2
Nb-Ti (Nb53-Ti47)	10	15
Niobium tin (Nb_3Sn)	18	24
MgB_2	39	12
$YBa_2Cu_3O_7$ (HTS)	92	~ 100
$Bi_2Sr_2CaCu_2O_{8+x}$ (HTS)	108	~ 100

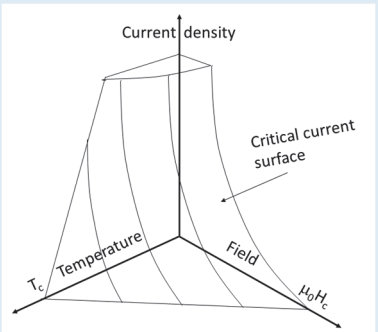

Having no electrical resistance (in DC conditions, see Box 7.4), superconductors can carry large electrical currents — wherein their interest for magnet builders. The power required for cooling is far less that than that which would be dissipated in resistive coils. Practical wires consisting of fine filaments of superconducting material embedded in copper (which stabilizes the conductor by providing a short-term parallel path for current) were first developed in the 1960s. They provide a very high current carrying capacity (~ 1000 A/mm^2), and led the way to an important increase in attainable magnetic field. The best understood and most used materials are the alloy Nb-Ti and the compound Nb_3Sn. Whereas Nb-Ti is strong and ductile, so wires and cables can be used directly for coil winding, Nb_3Sn is brittle, and coils with small radii of curvature, such as in accelerator magnets, must be wound prior to the heat treatment required to form the superconducting compound. Large-scale superconducting magnets were first built for high energy physics detectors (e.g. BEBC), and this tradition has been maintained with ever larger coils for collider experiments, e.g. ALEPH and DELPHI at LEP and ATLAS and CMS at the LHC. Coils for small and individually powered accelerator magnets can be wound using wire, but for the heavy currents adopted for series-connected magnets in large accelerators transposed cables are better [Highlight 8.2]. Flat cables that provide a good filing factor were developed for this purpose at the Rutherford Laboratory in the 1960s. Magnets for MRI constitute the most important commercial application of Nb-Ti; a large quantity of high performance wire was supplied for the LHC. Vigorous R&D on Nb_3Sn and High Temperature Superconductors (HTS) [Box 8.4] is underway for the next generation of accelerators [Highlight 12.3].

served as the inner wall of the helium vessel), the four main coils, a set of stainless steel spacers, a low-carbon steel yoke subdivided into four quadrants, five aluminium alloy rings shrink-fitted around the yoke, the outer shell of the helium vessel, the heat shield and the outer wall of the vacuum tank. The active part of the magnet, enclosed in the helium vessel, was cooled by natural convection in boiling helium at about 4.3 K and was suspended from the vacuum tank of the cryostat with four slender metallic rods of low thermal conductivity.

The main coils

In superconducting magnets the field is determined by the current in the windings. A pure quadrupole field is produced by current proportional to cos2θ distributed on a circle, θ being the polar angle. To be efficient the windings have to be as close as possible to the where the field is required. Taking into account the space for thermal insulation, correction windings and minimal clearance, the main coil had an inner diameter of 232 mm. The conductor was composed of about 1700 niobium-titanium filaments of 46 μm diameter embedded in pure copper, with cross-section 1.8 mm × 3.6 mm, and copper to superconductor ratio 1.5:1. The copper serves to support the fine filaments and to shunt the current in the event of a transition to the normal state (quench) for the time required to detect the fault and ramp the current down. A good approximation of a pure quadrupole field was found to be given by three blocks of conductors per half-quadrant, of constant thickness (38.5 mm) and uniform current density, separated by metal spacers as shown in Fig. 4.6. This configuration offers convenient surfaces for the transfer of forces between coils and clamping structure [23]. At operational field gradient, 45 T/m, the current was 1680 A and the peak field in the winding 6 T, approximately 6 times the strength of a typical superconducting MRI magnet used for medical imaging.

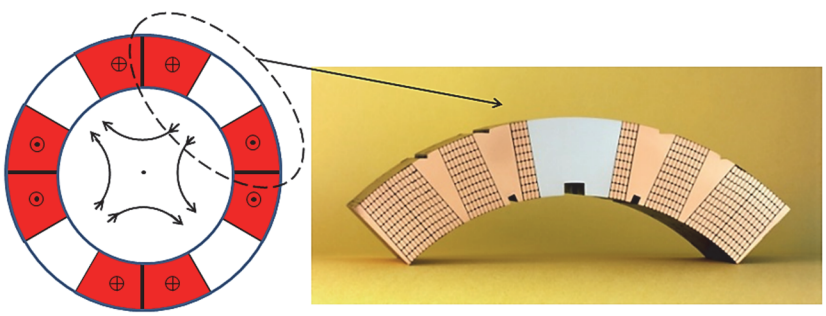

Fig. 4.6. Schematic cross-section of a quadrupole coil assembly and a cross-section of an actual quadrant showing conductors, stainless steel post and copper spacers.

The coil support structure

In operation, the main coils are subject to large electromagnetic forces (200 t/m length on each coil half). The coil support structure consists of the iron yoke and the aluminium shrinking rings. Besides providing a stiff support limiting deformation of the coils, the yoke limits the stray field and reduces the required excitation current.

In 1973, when the design of the superconducting quadrupole was started, the development of superconducting magnets of *circular* geometry (solenoids or similar) had already reached a stage where they could be designed with confidence. However, practically all magnet models *with straight-sided coils* necessary for handling high energy particle beams were plagued by degradation. In the light of this experience it was realized that a crucial difference between circular and straight-sided magnets lies in the way in which the electromagnetic forces are reacted by the structure. Sudden movements of even a few μm or microscopic cracks or slips occurring in the coil can generate enough heat locally to increase the temperature beyond the critical and cause the magnet to quench. The problem of mechanical stability was solved by the application of the principle of the Roman Arch [24]. The coil is compressed from outside, without support inside (Fig. 4.7), to prevent the appearance of tensile stress in operation. This concept, first applied intentionally to the ISR quadrupoles, has been generally adopted for superconducting magnets for accelerators.

A second objective of the project was to transfer superconducting magnet technology to European industry in anticipation of future projects. Effort was therefore put into preparing detailed specifications and manufacturing drawings, so that firms could estimate their costs and submit competitive tenders. Their responsibility would be to respect the choice of materials, dimensional tolerances,

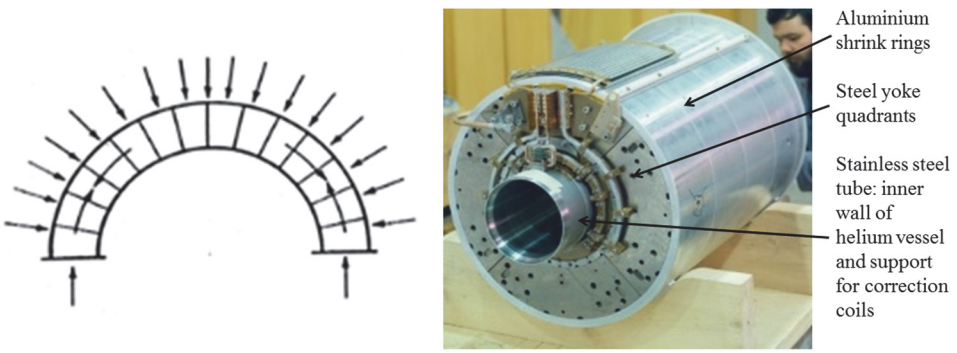

Fig. 4.7. Left: Roman Arch analogy — the elements of a Roman arch are maintained in compression. Right: an industrially produced quadrupole showing the major structural components.

and fabrication procedures, and to perform the checks and tests specified by CERN. CERN would take responsibility for performance. This project demonstrated by example CERN's strategy for the development of novel technology driven by cutting-edge research and for the procurement of components based on such technology: design, production and testing of prototypes at CERN until all the technical detail is understood, and then production in industry which has to meticulously follow the production steps and tolerances prescribed by CERN.

The manufacture of the 8 magnets took about two years. All magnets achieved the required performance [25]; there was no re-training or degradation after repeated thermal cycles from 293 K to 4.2 K. The insertions were installed at Point 8 of the ISR, to be used in combination with the Open Axial Field Magnet [Highlight 4.11], the centrepiece of a large detector [26]. Regular operation of the insertions started in 1981 and continued until the end of ISR operation in 1983. Luminosity was increased sevenfold, a record of 1.4×10^{32} cm^{-2} s^{-1} being reached for proton–proton operation. No quench of the magnets occurred during stable beam operation [27, 28]. Besides providing superb and unique experimental conditions for the researchers, the project led to an advance in magnet technology and allowed CERN to acquire expertise in the application of superconductivity and associated cryogenics that would prove to be invaluable in subsequent years.

4.5 Cryogenics for the Superconducting High Luminosity Insertion Magnets

Philippe Lebrun

The high luminosity insertion at Point 8 of the ISR [28] consisted of eight individually powered superconducting quadrupoles operating at currents of up to 2 kA in saturated helium baths at 4.5 K, housed in stand-alone cryostats [Highlight 4.4]. The cryostats also contained individually powered sextupole and 12-pole correction windings, also superconducting, and were equipped with corresponding current leads, as well as with room-temperature bores. The main challenge was to build, install and operate reliably — for the first time ever — a system of superconducting magnets with its ancillary cryogenics (see Fig. 4.8) in a functioning high energy accelerator, with minimum disturbance to the physics programme.

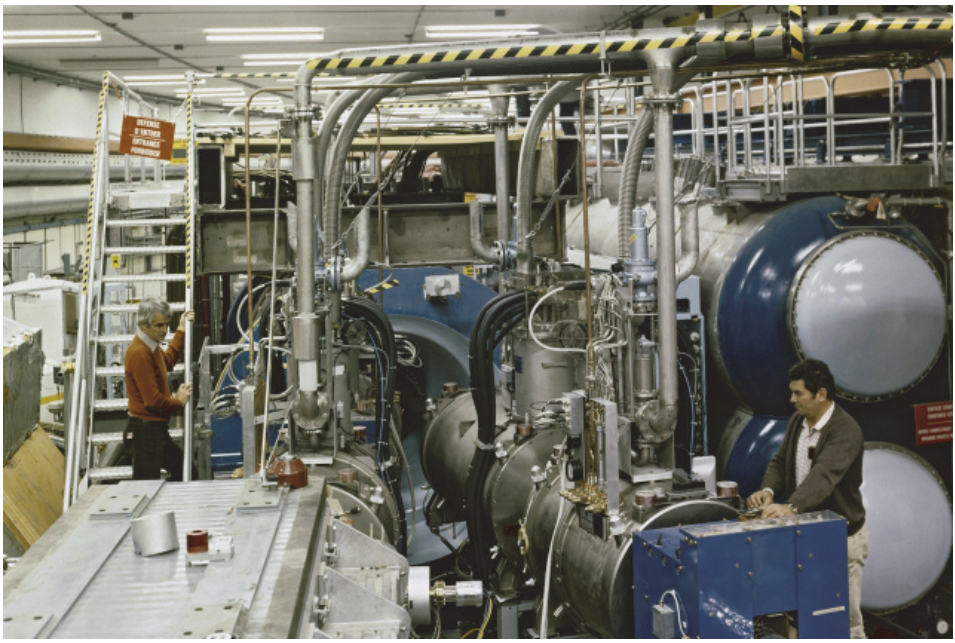

Fig. 4.8. The superconducting high luminosity insertion installed at Point 8 of the ISR.

Thermal optimization of the cryostats and cryogenic lines requires intercepting a large fraction of the heat in-leaks at higher temperature than 4.5 K, on thermal screens usually cooled by liquid nitrogen or cold gaseous helium. Rather than distributing the latter fluids in addition to the liquid helium filling the magnet baths, it was decided to feed the cryostats only with liquid helium, use locally the cold helium vapour boil-off to intercept heat on the thermal screens of the cryostat, cryogenic lines, and current leads, and return gaseous helium at room-temperature to the cryogenic plant, thus operating it as a liquefier rather than a refrigerator [29]. Although *a priori* less favourable from a thermodynamic point of view [30], this choice greatly simplified the cryogenic distribution, cryostat pipework and control system, thus reducing parasitic heat in-leaks, regaining overall efficiency and improving reliability. It also enables to decouple the "customer" cryostats from the cryogenic plant, which can then operate steadily liquefying helium into a dewar vessel acting as buffer.

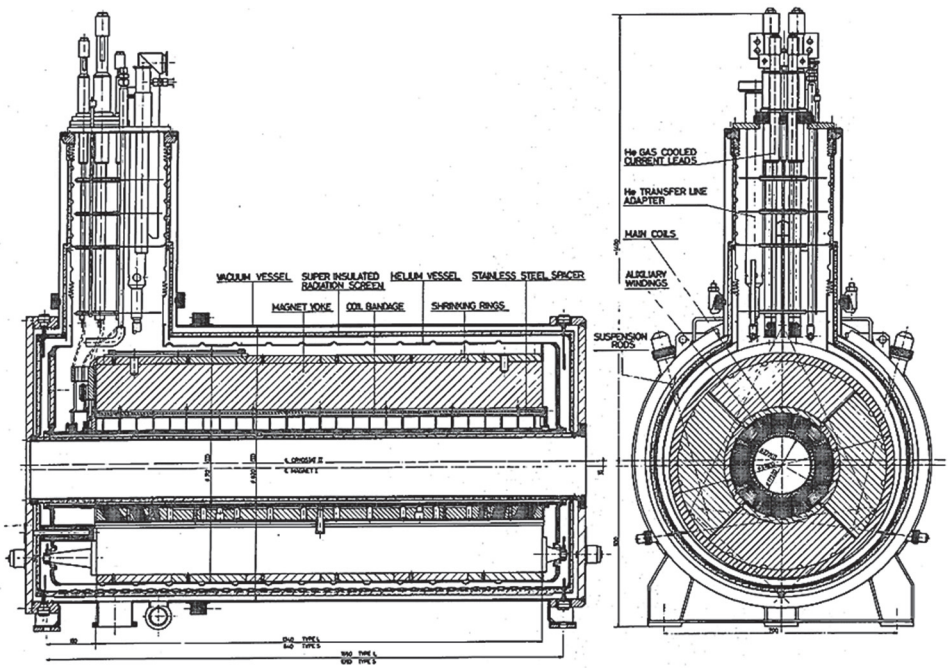

Fig. 4.9. Cross-sectional views of a superconducting magnet in its cryostat.

The cryostats (Fig. 4.9) were designed to fulfil their thermal, mechanical and magnetic functions, while being suitable for integration in the ISR. Technical solutions were chosen on the basis of their being adapted to manufacturing and assembly by industry, and their reliability in operation. The helium enclosure containing the magnet, made of AISI 304L austenitic stainless steel for the outer vessel and low-permeability AISI 304LN for the cold bore tube, was of an all-welded construction. It was surrounded by a radiation screen made of a hydro-formed, double-walled cylindrical shell of AISI 304L, wrapped with multilayer reflective insulation. The vacuum vessel outer shell was made of normal steel for shielding stray field, nickel-plated for surface protection, while the room-temperature bore tube used low-permeability AISI 316 LN. The cold mass was suspended from the vacuum vessel by four tie-rods made of Inconel 718, having four times lower thermal conductivity than standard stainless steel. The eight cryostats [31] were manufactured build-to-print and assembled by industry. Correct balancing of parallel helium vapour flows cooling the current leads was achieved by equipping them with compact, self-actuated thermostatic valves [32].

The cryogenic lines connecting the helium liquefier to the cryo-magnets in the ISR tunnel had to follow a contorted routing over a length of 50 m, imposed in particular by radiation shielding. Flexible multi-tube lines which could be entirely

constructed and leak-tested in industry, shipped coiled on transport drums and rapidly installed in the field thus constituted an attractive solution. Unfortunately, such products were not industrially available in the lengths and configurations of interest, but the company Kabelmetal (now Nexans) had developed and was exploiting a process (Wellmantel®) for the continuous manufacture of corrugated tubes in a variety of engineering materials, to be used as metallic envelopes of electrical cables and pipelines for residential heating. Prototype lines made of four nested corrugated tubes of austenitic stainless steel (Fig. 4.10) were developed in a collaborative spirit between the company and CERN [33]. Following excellent test results, the solution was retained and eight 50 m long lines were supplied and installed by the company [34, 35], in a fraction of the time and effort that the conventional rigid alternative would have required. Together with the rest of the cryogenic system, the lines operated smoothly from 1980 until the ISR was closed in 1984. They could also easily be dismantled and were reused in other locations, either permanently or for specific tests [36]. After 35 years, one of these lines is still in daily use at a CERN cryogenic installation!

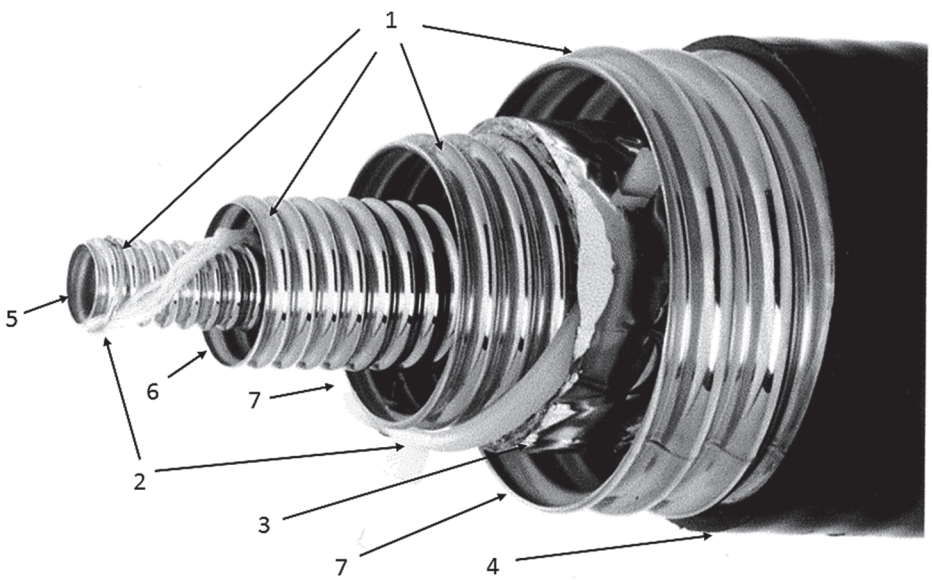

Fig. 4.10. Structure of the flexible helium transfer lines; 1: corrugated tubes; 2: helical-wound polyethylene spacers; 3: multilayer insulation; 4: polyethylene sheath; 5: liquid helium supply channel; 6: helium vapour return channel; 7: insulation vacuum space. (Photo: Nexans).

The cryogenic technology developed for the ISR superconducting high-luminosity insertions was later transposed to the LEP collider, thus enabling it to start operating from the onset with superconducting high luminosity insertions around its four large experiments [37], in spite of the very limited resources allocated to this part of the project. In the LEP experimental caverns, the superconducting quadrupoles were supplied in liquid helium by similar flexible lines of up to 92 m in length, spanning elevation differences of up to 25 m [38].

4.6 Van der Meer Scan: Proton Beam Tomography

Helmut Burkhardt

Knowledge of the luminosity L provided by a collider is fundamental. It quantifies the rate at which collisions occur. For a process of cross section σ, the collision rate N is given as the product $N = L\sigma$. In e^+e^- colliders, the luminosity can be determined to per-mille accuracy by measuring the rate of the Bhabha scattering process $e^+e^- \rightarrow e^+e^-$, for which the cross-section can be accurately calculated [39]. For hadron colliders the situation is more complex: there is no corresponding process with a well-known cross-section that can be used for calibration. A way out was pioneered at the ISR by Simon van der Meer (Nobel Prize 1984), who devised an ingenious method, now referred to as the "Van der Meer Scan" or "VdM" method [40].

The luminosity is determined by the flux of particles circulating in the collider, easily measurable as beam current, and the effective beam cross section, which is difficult to measure accurately. In the VdM method this cross section is measured by scanning one beam through the other (Fig. 4.11). The collision rates are recorded and plotted as a function of the relative displacement of the beams. The collision rate is at its maximum when the beams are colliding head-on, and decreases gradually when the transverse beam separation is increased. It can be shown that the effective beam cross section, irrespective of beam shape, is the area under the curve plotted divided by the maximum collision rate [40]. Varying the separation between the beams using magnetic steering is rather straightforward for machines in which particles of the same charge collide, such as the ISR, RHIC and LHC. A major strength of the VdM method is that beam profiles can be measured during physics operation, directly in the interaction region, which minimizes systematic uncertainties in the interpretation of experimental data.

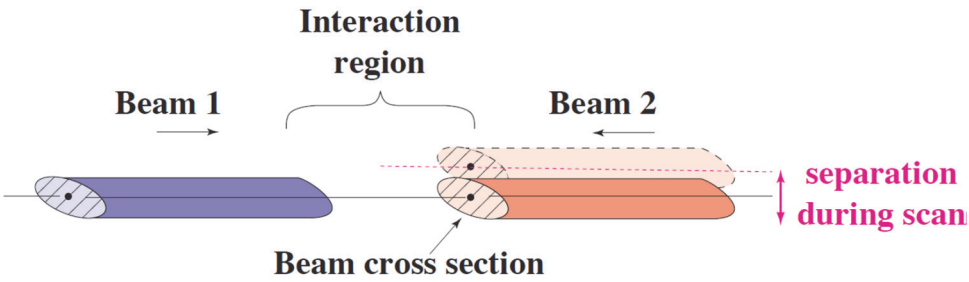

Fig. 4.11. Concept of the Van der Meer scan to determine the beam profile.

At the ISR the luminosity was determined with an accuracy of 1% [41]. This was helped by the fact that the ISR operated with continuous beams (not bunched), allowing absolute beam current measurements, and beam cross sections that were large enough for length scales to be calibrated precisely by mechanical means (using scrapers). For the Tevatron, which could not use the VdM method, the luminosity uncertainty was typically 15–20%.

The LHC renewed with the ISR tradition of VdM scans for determining luminosity [42] and optimizing the collisions [43]. After three years of operation, systematic uncertainties down to 1.5% have been achieved [42]. An automatic online procedure has also been developed for making VdM scans and directly sharing the results with the experiments [44]. The procedure includes a detailed analysis of beam dynamics uncertainties in VdM scans and has been adopted at both RHIC and the LHC. Automatic mini-VdM scans are now standard procedure in LHC operation and are used to optimize collisions for every physics run.

4.7 Roman Pots: Physics Next to the Accelerator Beam

Giorgio Matthiae

The “Roman pot” technique was invented at the ISR to study particles scattered at very small angles. These particles travel close to the circulating beams — in fact inside the vacuum chamber. They can only be detected by a special system able to place detectors a few millimetres from the beam. This system has come to be known as “Roman pots”.

One may wonder why it is interesting to detect particles scattered at very small forward angles. The main motivation was to find out how the total cross-section of the scattering of a proton on a proton depends on the centre-of-mass energy. This fundamental quantity defines the overall probability of interaction of the two colliding particles. The total cross section is related through the “Optical Theorem”

to the probability of elastic scattering of the protons in the forward direction. It is of course impossible to detect particles which are scattered precisely in the forward direction because they travel inside the beam; so what it is done is to measure particles scattered at very small angles and extrapolate to the forward direction. Using the Roman pots, the first experiments at the ISR made the startling discovery that the proton–proton total cross-section increases at the new energies probed by the ISR.

The basic theoretical ideas on the energy behaviour of the total cross section are discussed in [45] while the ISR measurements are described in [46, 47].

The Roman pots are special, movable sections of the vacuum chamber which contain small detectors. They are connected to the main vacuum chamber of the collider by bellows (Fig. 4.12, left panel), which are compressed as the pots are pushed towards the beam circulating in the collider. In their retracted position, the Roman pots do not obstruct the beam, thus leaving the full aperture of the vacuum chamber free for the beam during the injection process when the beam is very wide. Once the collider reaches its coasting energy with stable beams, the Roman pot is moved towards the beam with the aim of getting as close as safely possible.

Why Roman? This is because they were first used by the CERN-Rome group in the early 1970s to measure the total cross section at the ISR. And why pots? A picture of the first Roman pot used at the ISR is shown in Fig. 4.12, right panel. It was of a rather simple design, its rounded shape being at the origin of the name. When the physicists of the CERN-Rome group first proposed to use the pots, several people said that they were insane, because the inside of the vacuum chamber is a very inhospitable place, and it would be impossible to perform sensible experiments.

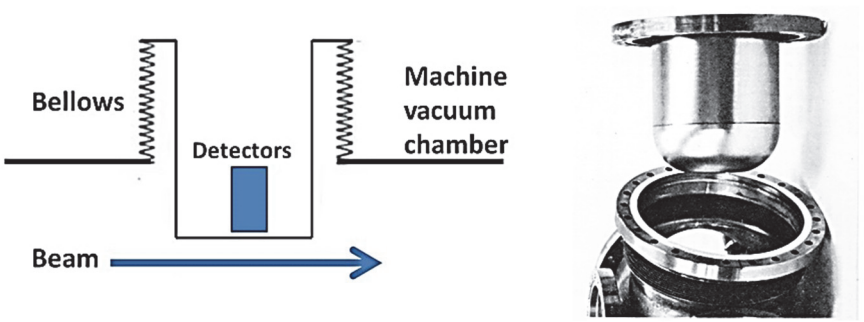

Fig. 4.12. Left: the concept of the Roman pot. Right: the first Roman pot used at the ISR.

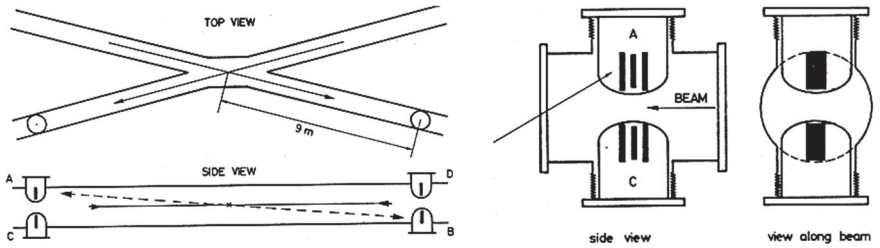

Fig. 4.13. Left: the two pairs of Roman pots of the CERN-Rome group were installed at the end of the ISR straight section, i.e. at about 10 m from the crossing. Right: sketch of the pots and of the detectors which could be approached to about 10 mm from the beam axis [47].

Connected with bellows to the vacuum chamber, a single Roman pot would be pushed strongly by the atmospheric pressure, increasing the difficulty of precise positioning with respect to the beam. This problem was solved by connecting mechanically the pots on either side of the chamber, bringing them into a nearly balanced state (Fig. 4.13).

Operation of the Roman pots required very close collaboration between the experimentalists and the machine physicists. It was crucial to have stable beams with minimal transverse haloes. Such very clean beams, resulting in very low background for the experiments, were obtained by "scraping", by inserting a thin absorber inside the machine vacuum chamber slowly and carefully — a simple but effective technique to remove the tails of the particle beams. By removing the tails it was possible to approach the beam, placing the pots within a few millimetres — in the best conditions at only 9 mm from the beam axis. This operation had to be repeated several times during a data-taking period because the tails of the beam built up again gradually after the "scraping" due to scattering of the circulating particles against molecules of the residual gas. In fact, a good, clean beam turned out to be the way for the detectors to work in the ferocious environment close by.

After the ISR, Roman pots were used at the CERN p–$\bar{p}$ collider (Fig. 4.14), at the Fermilab Tevatron collider, at the DESY electron-proton collider, and are currently used by the TOTEM experiment at the CERN LHC proton collider.

The detector technique evolved with time, as required by the physics of elastic scattering at the new accelerators of higher energy [49]. The space resolution was of the order of 1 mm for the scintillator hodoscope at the ISR, of about 100 μm for the drift chambers at the SPS collider and eventually became as small as 10 μm for the Si microstrip detectors of TOTEM at the LHC [50].

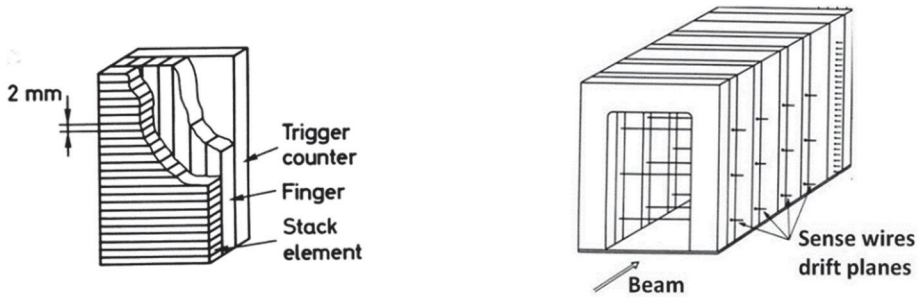

Fig. 4.14. Left: the small hodoscope of scintillation counters used by the CERN-Rome group at the ISR. Right: sketch of a special drift chamber used by the UA4 group at the CERN p–$\bar{p}$ collider. The U-shaped frame of the chamber allowed the sensitive region of the chamber to approach the beams to within a few mm. An improved pot with a flat bottom plate was used for this experiment [48].

4.8 The Gas Detector (R)evolution

Fabio Sauli

The physics models current at the time of the conception of the ISR favoured the design of experimental setups optimized for detection of particles generated by proton-proton collisions in the forward direction. This required a detector design capable of bringing the sensitive area as close as possible to the vacuum chamber of the machine, and able to handle very high particle fluxes. None of the devices used in the sixties could meet these requirements. The invention in 1968 at CERN by Georges Charpak of the Multi-Wire Proportional Chamber (MWPC) [Box 4.4] completely changed the scenario [51]. Capable of detecting and electronically recording particle positions at a high rate, and permitting the coverage of large areas, they could be tailored to be sensitive a few cm from the vacuum chamber. It started a revolution in particle physics, recognized with the Nobel Prize to Charpak in 1992. The choice of this novel technology as main tracker of the Split-Field Magnet Detector (SFMD) was natural, albeit daring. A large-size MWPC prototype built by Charpak and collaborators is shown in Fig. 4.15 [52].

The original MWPC design, making use of heavy frames to tension and hold the stretched wires, was found to be ill-suited for installation within a magnet, where the ratio of sensitive to total detector area is a premium. An alternative assembly offered a much improved aspect ratio: light honeycomb plates tailored to cover the sensitive area, with the wires soldered to slender frames glued to the support plates [53]. This structure is very light and easy to handle, and has since been used for a large number of experiments.

Multi-wire proportional chambers **Box 4.4**

The multi-wire proportional chamber (MWPC), is a gas-filled radiation detector made with a grid of parallel and closely spaced thin metal wires (the anodes) stretched between two electrodes (the cathodes), see figure below. The typical wire spacing is one to few millimetres with a distance between cathodes of the order one cm. On application of a voltage between the electrodes, electrons released in the gas by ionizing radiation drift towards the anodes, where in the increasing electric field they collide with and ionize the gas molecules, resulting in charge multiplication, in a process called an electron-ion avalanche.

Even though multiplication factors of several tens of thousands can be reached in most gases, in order to detect small ionization yields it was necessary to use rather expensive electronics. This requirement made it problematic at the time to implement the large systems needed for particle physics. Discovered by Charpak and collaborators, filling with so-called "magic gas", a mixture of three or four component gases, permitted to reach gains above a million, and was paramount in the choice of the technology to equip the first large all-electronic detectors.

The MWPC localization accuracy, limited by the wire spacing of one or two millimetres, can be improved by an order of magnitude by measuring the charge distribution induced by the ion avalanches hitting the suitably segmented cathode planes.

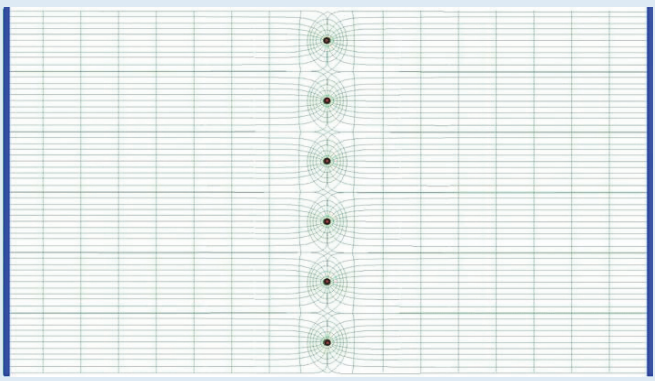

MWPC schematic showing electric field lines between anode (centre) and cathode wires (sides).

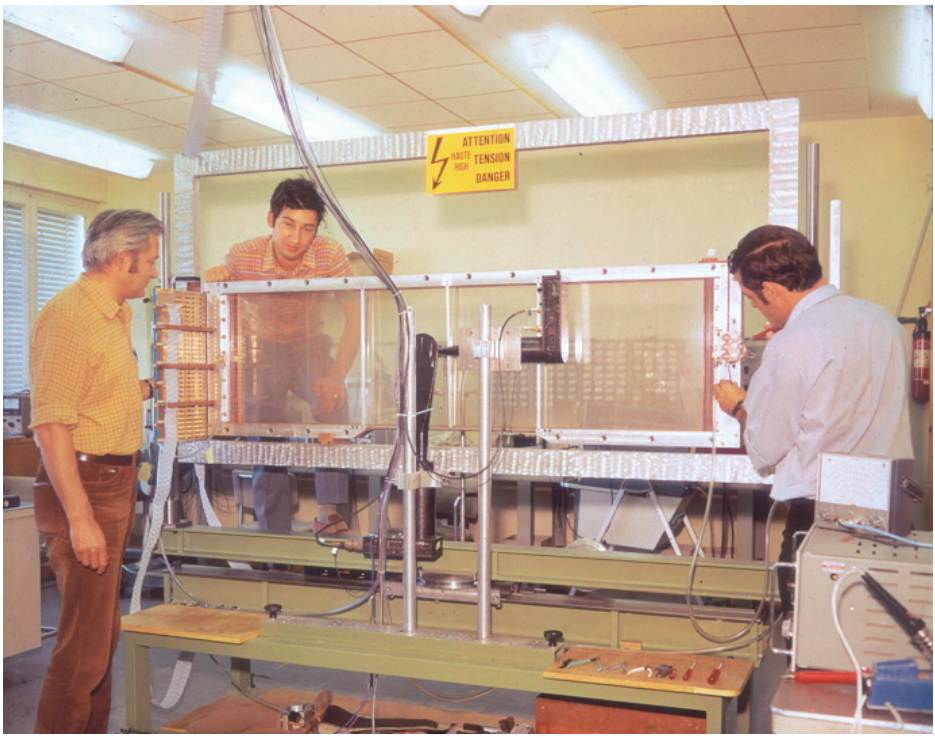

Fig. 4.15. Georges Charpak (left) and collaborators with one of the first large MWPCs.

A system of 40 MWPCs of this light-weight design with around 50,000 sense wires and the electronics to read the signals was completed in record time, and in 1972 the SFMD was ready to take data (Fig. 4.16). With one coordinate provided by the wire hit, and a coarser information given by pickup strips on the cathode planes, the detectors provided two-dimensional space points for the measurement of particle momenta from their bending radius in the magnetic field. The SFMD took data along the operating lifespan of the ISR, producing many results of relevance for fundamental physics.

The quest for free quarks, one of the physics motivations to build the ISR, was not successful, despite the demonstration that the single-electron sensitivity achieved using the "magic gas" filling permitted to efficiently detect the hypothetical particles. It became clear later that "confinement", a fundamental property of the strong interaction, prevents the existence of free quarks and hence their direct observation in the laboratory.

There were many derivatives of the revolutionary MWPC concept. In one frequently used form the drift time between the passage of a particle and the arrival time of the ionization charge on the anode wire is measured, providing much improved position information. These "Drift chambers" were widely used at the ISR [Box 4.5], the most advanced version being constructed for the Axial Field Spectrometer (AFS), shown in Fig. 4.17 [54]. Two half-cylinders around the central beam pipe were immersed in the field of the Axial Field Magnet [Highlight 4.11]. The full azimuth was subdivided into 4^0 cells, each one being instrumented radially with 42 anode wires, measuring the drift time. This very high subdivision was instrumental in imaging events with highly collimated groups of particles. These were some of the first observations of "jets", the incarnation of quarks and gluons expelled from confinement.

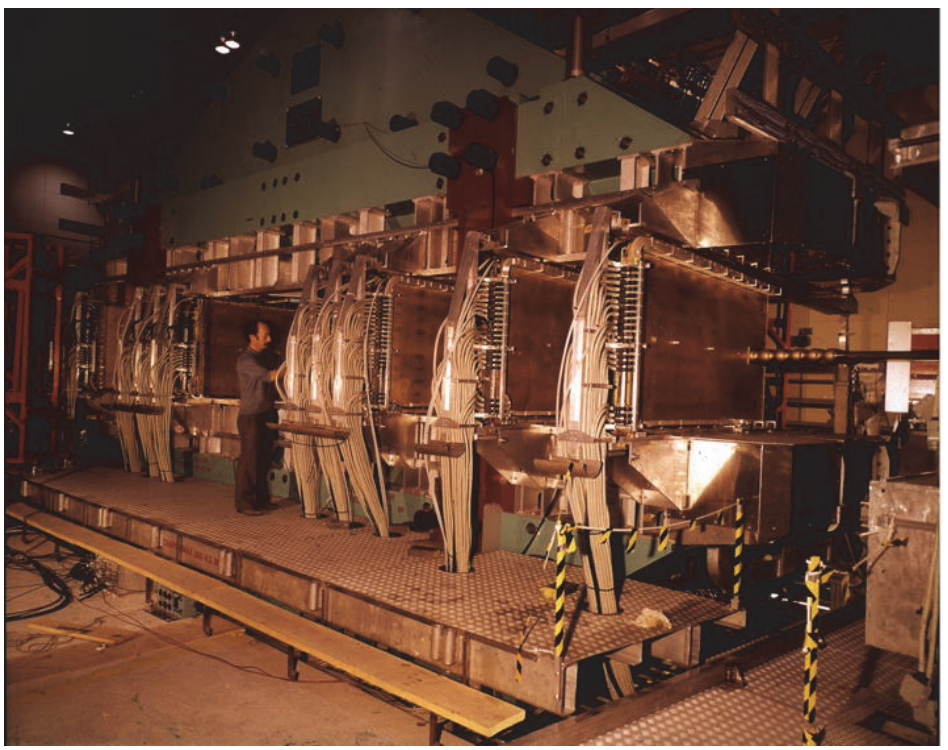

Fig. 4.16. The Split-Field Magnet Detector with the MWPCs of the novel light-weight design installed between the poles of the magnet.

Multi-wire drift, imaging and time projection chambers **Box 4.5**

A measurement of the time taken by the electrons released in the gas to reach the anodes, together with a precise knowledge of their drift velocity permits to infer the distance of the track from the wires with sub-mm accuracy. Developed in a wide variety of designs, from planar to cylindrical structures with cell sizes of several centimetres, multi-wire drift chambers provide localization accuracies of a few hundred microns or better with a relatively small number of measurement channels. Examples of large drift chamber systems are the cylindrical AFS detector used at the ISR (see main text), and the UA1 imaging drift chambers at the CERN proton-antiproton collider [Highlight 6.5].

In the time projection chamber, first used at SLAC and then in two LEP experiments and presently in ALICE at the LHC, the sensitive volume is a large gas vessel where ionisation trails are produced by the particles; the vessel is instrumented at one end with MWPCs. A measurement of the drift time gives the distance of the tracks from the wires, while a recording in short time intervals of the charge induction profiles on one cathode, stripped or padded, provides the other two orthogonal coordinates.

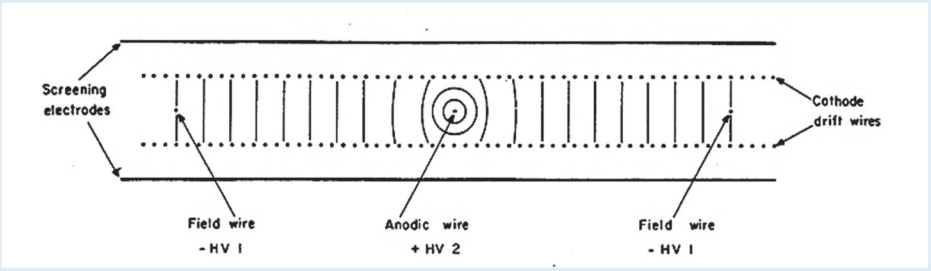

Schematic drawing of the high accuracy drift chamber.

Widely used in particle physics experiment and other applied research fields, MWPCs have several intrinsic drawbacks. The slow positive ions created in the multiplication process accumulate in the drift volume, causing field distortions and efficiency losses at high radiation fluxes; more serious, the formation in the avalanches of molecular aggregates of the main gas or of pollutants, coating the thin wires, results in permanent damages after long exposure to radiation (a process called "ageing"). A new family of gaseous devices, named micro-pattern gas detectors, (MPGD) solves many of these problems [55]. One frequently used detector in this family is the gas electron multiplier (GEM) [Box 4.6] introduced in 1997 [56]. Manufactured with a high-quality printed circuit technology developed at CERN, GEM electrodes can be tailored to the experimental requirements, and assembled using light yet sturdy honeycomb supporting frames.

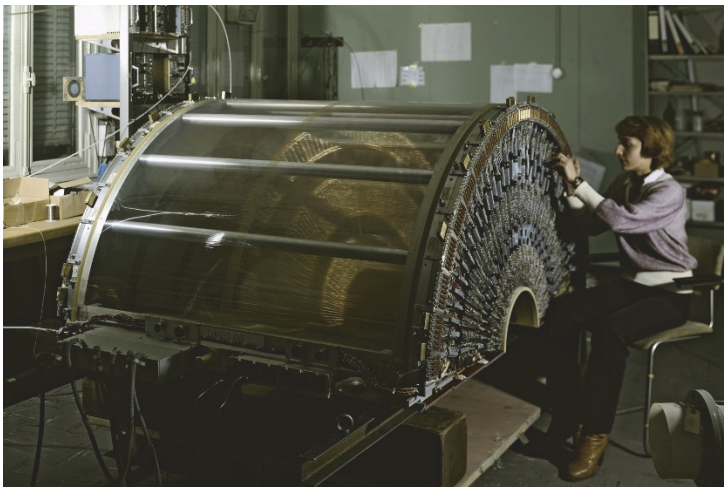

Fig. 4.17. One half of the AFS cylindrical drift chamber. The anode and cathode wires were strung coaxially with the beam between the endplates, which carried the readout electronics.

The Gas Electron Multiplier (GEM) **Box 4.6**

Introduced in the late nineties, the gas electron multiplier (GEM) provides charge amplification in closely spaced narrow holes, typically fifty to hundred per square millimetre, etched on a metal-clad polymer foil with a photolithographic process. Electrons released in the upper region drift downwards into the high field of the holes, multiply and proceed towards the lower region; unlike other gaseous counters, the charge amplified by a GEM foil can be multiplied further in one or more cascaded electrodes, permitting to safely attain very large overall gains and reach single electron detection. Owing to their high granularity, GEM detectors are efficient at very high radiation fluxes, and achieve excellent spatial localization and multi-track resolutions.

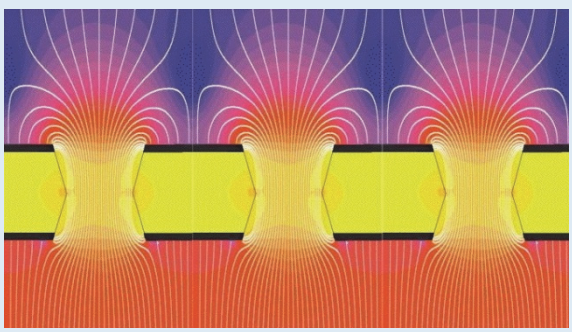

The electric field lines in the holes of a GEM electrode.

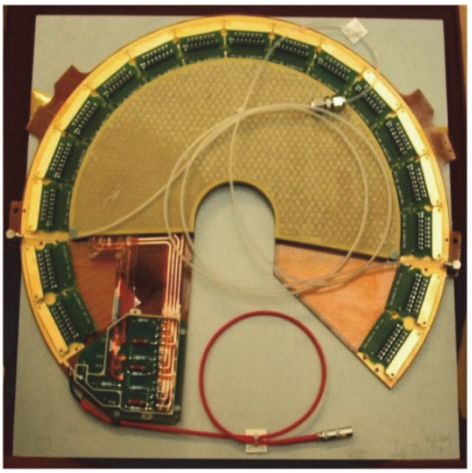

Fig. 4.18. A half-moon shaped GEM detector complete with its readout electronics.

Several hundred electrodes of this design have been produced at CERN for the construction of the tracker in the COMPASS spectrometer. Installed in 2001, the tracker is still in operation, demonstrating the reliability of this new detector technology. Figure 4.18 shows the half-moon shaped module developed for the TOTEM forward tracker.

Because of their superior performance, GEM detectors are foreseen to gradually replace wire-based devices in LHC experiments, e.g. the ALICE TPC end-cap MWPCs and the CMS muon detector, in order to better cope with increased interaction rates. Many other applications in medicine, biology, plasma diagnostics, neutron imaging are under development [56].

4.9 Transition Radiation: Imaging Relativistic Particles

Christian Fabjan

In the early years of research at the ISR the view emerged that «new» physics phenomena might reveal themselves through the observation of leptons, i.e. electrons and muons, not explainable with conventional physics. Such textbook examples are the discovery of the J/Ψ or the rare pion decay [Highlight 2.3]. But Nature likes to be cagy about revealing its secrets: These “new physics” leptons would be produced very rarely, if at all, and are difficult to detect. The ISR R209 collaboration, led by the co-discoverer of the J/Ψ and Nobelist S. Ting, developed a large Muon Spectrometer for this purpose. The R806 collaboration placed its bet on electrons. The stakes were high enough, daring the collaboration into

developing two novel — most physicists thought exotic and unrealistic — detector concepts: Liquid Argon Calorimetry [Highlight 4.10] and Transition Radiation Detectors (TRDs).

Transition radiation (TR) is a close relative of Cherenkov radiation (CR) [Highlight 7.8]. When an ultra-relativistic particle transits from one medium to another, its own electric field and the atomic electrons in the new medium are affected. The particle reacts to this abrupt change of electric fields by "shaking off" photons, "Transition Radiation", which is emitted over a wide frequency spectrum, ranging from visible light to soft X-rays of some tens of keV. Like CR, TR is an electromagnetic effect. Its theoretical description is subtle and has occupied a generation of physicists, thanks to which it can now be precisely calculated. These changes of field extend over a characteristic length of some fractions of a millimetre along the particle trajectory. This must be taken into account in designing such TRDs. In contrast to CR, which is a function of the particle velocity v, TR is a function of $\gamma = \{1 - (v/c)^2\}^{-1/2}$, c being the velocity of light. Radiation in the X-ray domain starts to be emitted effectively only for particles with $\gamma > 1000$, i.e. $v > 0.999\ 999\ 5c$. At the ISR the only particles produced with such large γ-values are electrons, making TR the technique of choice for the identification of these messengers of "new physics". A detailed experimental verification of the theory was made at CERN, placing the development of the TR Detectors (TRD) for R806 on solid ground [57].

TR is quite a feeble process: the probability of emitting a photon of a few keV in passing through one such transition is calculated to be at the percent level. How can such a small effect be turned into a practical particle detector for large solid angle experiments? It requires the particle to traverse hundreds of interfaces between the two different media, still only producing a modest signal of a few X-ray photons. The photons are emitted close to the particle trajectory and must also traverse these material interfaces, before being measured in a suitable X-ray detector. None of these ingredients were available at the time. The theoretical optimization indicated that the required few hundred interfaces could be realized with foils, typically tens of microns thick, spaced by some hundreds of microns. To make use of all these foils the "Radiator" material must have a very high transmission probability for X-rays. Thin beryllium foils are the best, but are poisonous and difficult to handle. Next best is lithium, but this is hygroscopic and inflammable. Other materials are less performant. The collaboration considered the difficulties in making lithium radiators to be surmountable: it would require very dry air for the assembly, and an inert atmosphere (e.g. helium) for subsequent use in the experiment. A dry lab with relative humidity < 3% would not be difficult to set up — had it not been for the CERN Safety Group, concerned about the health

risks associated with working in such an atmosphere over extended periods. Luckily, the US Air Force had previously studied the effect of dry air on pilots and found they performed better, without their health being affected! That settled the safety issue of radiator assembly, but the X-ray detectors had still to be developed. Given the large areas required (about 10 m^2), some form of a gas detector, such as MWPCs, was a plausible choice [Highlight 4.8], but this would require finding a gas which absorbs the X-rays efficiently. Xenon was found to be best: in such Xe-filled MWPCs the TR photons, when absorbed, produce one or more "photo-electrons", which deposit their energy through ionization in the MWPC. In this way all or most of the energy of the incident TR-photon is converted to ionization. However, in addition to this ionization the traversing relativistic electron also ionizes the gas in the chamber, and the signal recorded is the sum of the two processes. The much more abundant but heavier charged particles, e.g. pions, protons, do not produce TR photons so their associated signal is very much smaller than that of electrons. Tests were performed to confirm calculations which had indicated that in such an arrangement electrons could be clearly distinguished from the other more abundant particles.

In the experiment (Fig. 4.19) each of the particles produced in a collision traversed two such detectors to increase the quality of electron identification, with less than one percent of charged pions mistaken for electrons. Measurement of the

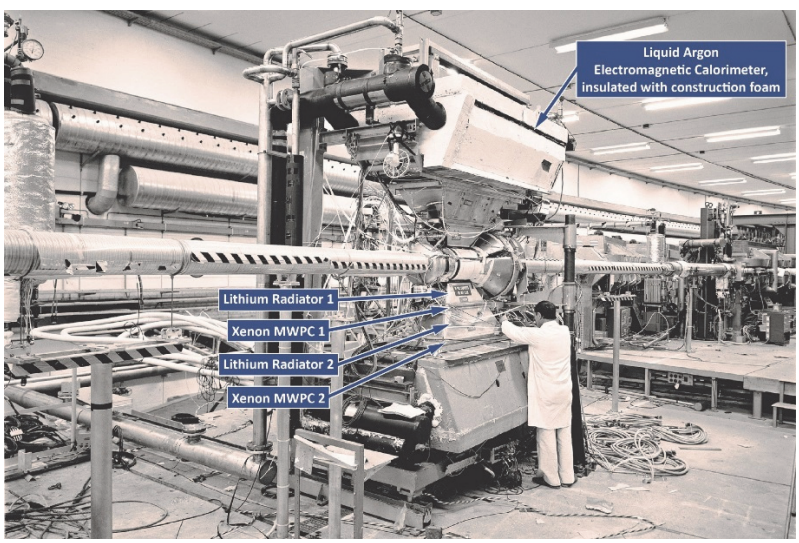

Fig. 4.19. Initial test set-up of the R806 collaboration to demonstrate the feasibility of Transition Radiation and Liquid-Argon calorimetry.

energy in an associated calorimeter provided further discrimination lowering the level of miss-identification of pions to 10^{-4}. This was sufficient for the physics research, but came six months too late: the ISR had missed the discovery of the Upsilon meson, made at Fermilab in the summer of 1977.

Following the R806 demonstration of TRDs, this technique became widely used whenever electron identification was at a premium [58]. The UA2 and UA6 collaborations at the p–$\bar{p}$ collider built such instruments; the NA31 collaboration used this technique in its pioneering CP violation experiment [Box 3.3]; the NA34 collaboration at the CERN SPS took the concept one step further, combining eight sequential, rather compact TRDs to form an electron identifier with tracking capability. A novel geometry of detector chambers allowed to distinguish electronically between the continuous ionization along the track and localized energy deposit of the X-rays, further improving the electron-pion discrimination. The NOMAD collaboration developed a large system for electron identification to study neutrino interactions. The technique found its way into the HERA collider at DESY, the p–$\bar{p}$ collider, the Tevatron, at Fermilab and the e^+e^- collider, Tristan, at KEK in Japan. And the LHC experiments employ this technique on a grand scale. The ATLAS collaboration built the "Transition Radiation Tracker", TRT, using an ingenious geometry to track charged particles with bubble-chamber like detail and to simultaneously identify electrons.

Left: one of the 18 modules of the ALICE TRD.

Below: the radiator consists of mats of polypropylene.

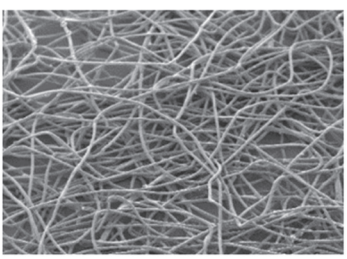

Fig. 4.20. One of the 18 modules of the ALICE TRD during final tests prior to installation. Six radiator-detector layers are contained in such a module. The last layer seen in the photo shows the signal and real-time trigger electronics, directly behind the X-ray detector. The radiator (insert) is made for technical reasons from mats of polypropylene fibres. (Source: University of Heidelberg).

The ALICE collaboration developed the NA34 concept further, building the world's largest TRD (Fig. 4.20) and using novel signal processing techniques to enhance the TR-signal and to identify electrons in real-time for event selection [Highlight 8.11] in a daring — yet successful — tour-de-force [59].

These detectors are now also making an impact in astrophysics, the most spectacular application being the choice of a powerful TRD as a key component of the Advanced Magnetic particle Spectrometer, AMS, based on the International Space Station, ISS. This experiment studies with superb detail features of cosmic rays, with an emphasis on antimatter.

4.10 Precision Calorimetry: Honing an Essential Tool

Christian Fabjan

Calorimetry, the energy measurement of particles, is ubiquitous in modern particle physics experiments, as explained in the Box 6.3. Conceptually, a calorimeter is a block of material, in which an incident particle is absorbed by transferring its energy through sequential interactions to a "shower" of lower energy particles. Measuring the sum of the energy of the shower particles gives the energy of the incident particle. In the early 1950s this technique was pioneered for the detection of *electrons* in the Nobel-prize winning determination of the size of the proton in the famous electron scattering experiments by Hofstadter at SLAC. In the early 60's the technique was extended to detect *hadrons* in cosmic rays. Experiments with calorimeters at the CERN SC and PS, and in other laboratories followed. Some of the first generation ISR experiments required large arrays of photon or electron/positron calorimeters [9].

Calorimetry became a focal point of detector R&D at the ISR with the emergence of experimental concepts requiring a high quality energy measurement of particles [60]. Part of the motivation came from the nascent ideas of the Standard Model of particle physics with its force carrier bosons, revealed in decays into electrons, muons and neutrinos. Neutrinos can of course not be measured directly, but their energy can be inferred. At an electron-positron collider the sum of the particle momenta is zero before and, by conservation, also after the collisions. At a proton–proton (antiproton) collider the components of momenta and energy transverse to the direction of the beams are zero. A sufficiently precise measurement of the energy balance, e.g. summing the energy components in the plane transvers to the collision, should add up to zero. A neutrino will manifest itself as an unbalance in this transverse energy distribution.

In the quest for precision calorimetry two lines of R&D were pursued: understanding the underlying detector physics determining the intrinsic

performance, and developing instrumentation which would reach this performance while allowing the construction of apparatus that englobes the collision point quasi-"hermetically".

The physics of the absorption process depends on the particle type. Electrons (positrons, photons) interact via the electromagnetic, hadrons through the strong interaction (and also electromagnetically, if charged). These processes are quite distinct, leading to different optimizations and instruments for electrons and hadrons. Both breeds of calorimeters come in a large variety, depending on the way the absorbers are instrumented to extract the energy information.

In materials of high atomic number Z the electromagnetic (e-m) shower is very compact compared to the hadronic one: a 100 GeV-electron can be absorbed in some 20 cm of material, while a 100 GeV hadron needs an absorber 1 m to 2 m thick. Therefore, high-quality electromagnetic calorimeters (EMCs) can be built, where the absorber also functions as the particle detector. One example, extensively used at the ISR, is glass enriched with lead, "lead-glass". More recently, certain crystals have been specifically engineered to meet the experimental requirements [Highlight 8.8].

Besides this special class of homogeneous crystal EMCs calorimeters used at accelerators can be of a "sandwich" construction: suitably chosen absorber plates alternate with layers of an active detector medium, which provides a signal related to the absorbed energy (Fig. 4.21). In these devices only a fraction of the total energy is absorbed and measured in the detector medium, potentially an overriding limitation. Plastic scintillator plates were the detectors of choice: they are relatively cheap, easy to handle and provide a sufficiently strong light output to be

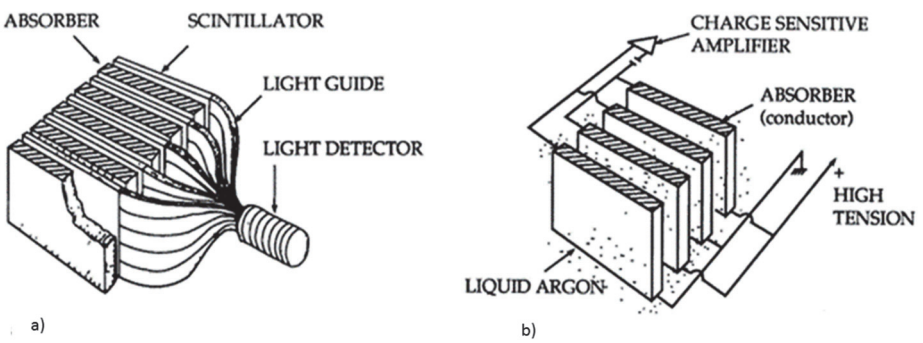

Fig. 4.21. Schematic of frequently used calorimeter readout techniques. (a) Plates of scintillator optically coupled to a photomultiplier. In modern instruments more compact readout methods of the scintillator light are used; (b) Ionization charge produced in an electron-transporting medium (e.g., liquefied argon) is collected at electrodes that also function as the absorber plates.

registered with photon detectors (Fig. 4.21a). The downside is that the photons are easily "lost", being absorbed in the scintillator or not recorded. The relation of the photon signal relative to the energy of the particle depends on many parameters, as does the signal of photomultipliers, requiring extensive calibration procedures to relate the signal to the energy.

The instrumental disadvantages of scintillators led to the unconventional suggestion to replace the scintillator with liquefied argon (LAr), an inherently stable medium. In LAr the charged particles of the cascade produce an ionization charge sufficiently large to be well measured (Fig. 4.21b) [60]. As Argon is used on an industrial scale it is amazingly cheap: a litre of LAr is cheaper than a litre of beer! This technique also offered a further, decisive advantage: the individual contributions to the energy resolution due to the construction and readout and due to the intrinsic physics effects could be identified and separately measured [61]. These advantages come at a price: LAr needs to be cooled to about 88 K, using liquid nitrogen, requiring a cryogenic installation. A view of the initial test device is shown in Fig. 4.22. This technique has found its way into many particle experiments. It has become the detector of choice for neutrino physics: a 700 ton LAr detector is operational; plans for 100 000 ton neutrino detectors are on the drawing board. Sometimes more exotic versions of this technique, using liquid krypton [Highlight 5.6] or liquid xenon are justified on performance grounds.

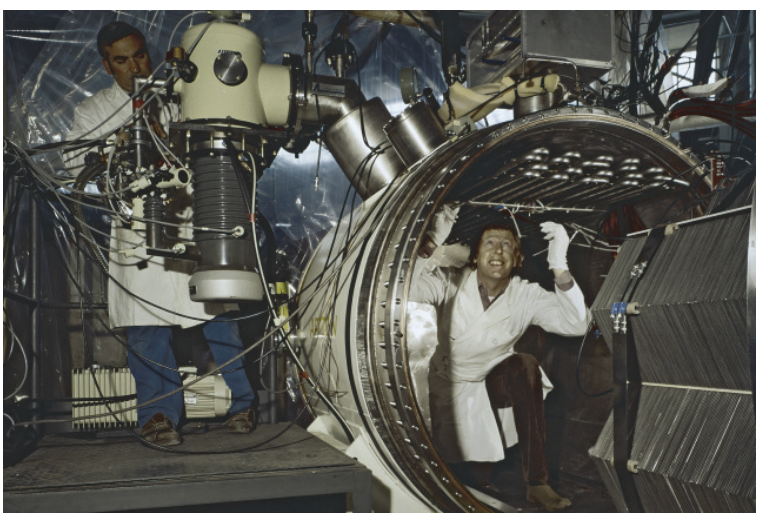

Fig. 4.22. Preparing for the first major liquid argon calorimeter test: a technician is preparing the cryostat prior to insertion of the calorimeter module on the right, consisting of 2 mm thick metal plates alternating with 2 mm gaps for the liquid argon. Liquid nitrogen is used to liquefy argon via a heat exchanger (stainless steel spiral).

Understanding the physics of the hadronic cascade and the *intrinsic* performance of hadronic calorimeters (HCs) turned out to be the real challenge [61]. It required measurements to isolate different contributions affecting the performance. Crucial input was given by novel computer simulations of the complex physics of the hadronic cascade at the individual particle and collision level. In these showers a vast range of particles is produced. High energy hadrons generate energetic secondary hadrons, but also break up (fission) the nuclei producing many low energy photons and neutrons. Energetic neutral pions are produced, which decay into photons, initiating an e-m cascade. These varied particles tend to be recorded with different signal strength in the active detector medium. This detailed understanding opened the door towards precision hadron calorimetry: it is crucial to equalize the calorimeter response to the electromagnetic and hadronic parts of the cascade.

Among the proposals to achieve this equality ("compensation") the most unconventional one was surely the suggestion to use depleted uranium 238 as absorber plates, left over from the production of fuel elements for nuclear reactors. Calculations, confirmed by measurements, showed that the particle-induced fission in these plates by the hadronic cascade produces additional particles, whose energy is detectable in the detector medium. Remarkably, this additional signal can be tuned to contribute just at the right level to achieve the desired compensation. The improvement in intrinsic energy resolution is a factor of 2, which for ISR experimentation was important. A 300 ton uranium scintillator calorimeter with full azimuthal coverage was constructed for the Axial Field Spectrometer [Highlight 4.11] [62]. These U-HCs measure a 10 GeV pion with a relative accuracy of some 6%, a 100 GeV hadron with a respectable 2%. It permitted the first observation at the ISR — concurrent with experiments at the CERN p–$\bar{p}$ collider — of "hadronic Jets": these are collimated sprays of particles, the manifestation of highly energetic collisions between the constituents of the protons, and crucial confirmation for the newly-developed theory of strong interactions. This concept was taken a step further at the electron-proton collider HERA at DESY, where the physics required the best HCs possible.

Imaginative applications of the calorimetric techniques have opened new fields in astronomy, studying the highest energy phenomena produced in cosmic accelerators [61]. In the search for the putative "Dark Matter" particles calorimeters are optimized for very low energy deposits. In medical diagnostics tumours are detected with Positron Emission Tomography, using crystals, similar to those used in the Higgs-Boson discovery [Highlight 10.4].

4.11 The Open Axial Field Magnet: Barrier-Free Access

Thomas Taylor

During the discussions in 1976 on a new facility for the ISR much emphasis was put on the importance of "openness" — both for minimising material in the path of particles produced by the collisions, and to allow good access for installation and maintenance of detectors during the short time allocated between runs. This led to the novel proposal of a normal conducting magnet, providing better access than either the superconducting solenoid or the toroid that were being discussed.

The concept was seized upon to figure in the proposal for an experiment presented in January 1977. By then basic field calculations and cost estimates for the Open Axial Field Magnet (OAFM) had been prepared, and it was confirmed to be an interesting alternative to the superconducting option. The field was lower, but it was shaped to be more efficient for momentum measurements than in a regular solenoid, the access was far better, and the cost would be less by a factor of 5. The design was optimised and the experiment was approved in March 1977. The magnet with its dimensions and field shape is shown in Fig. 4.23. The field is cylindrically symmetric out to a radius of 1.5 m, simplifying analysis of particle tracks. Small dipole and skew quadrupole correction magnets were installed close by to render the OAFM transparent for the circulating beams.

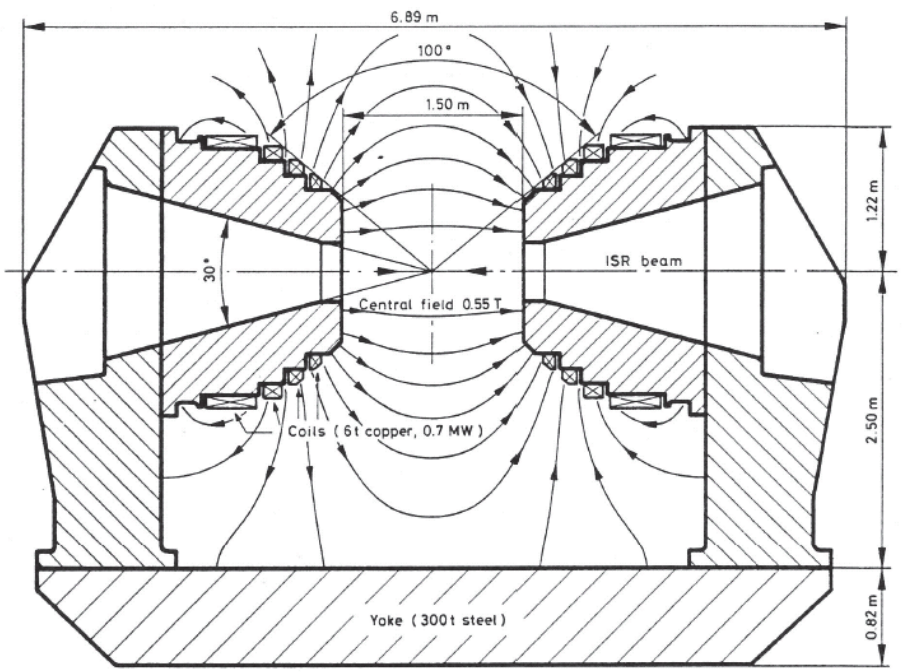

Fig. 4.23. Longitudinal cross-section of the OAFM, showing dimensions and field lines.

The field, 0.55 T at the centre, is produced by circular water-cooled copper coils clamped to hollow conical steel poles; it provides free access through azimuthal angles 0° to 15°, 40° to 140°, and 165° to 180°. The pole separation is 1.5 m. The magnetic flux is returned from the poles via cast low-carbon steel upright pieces, shaped to optimise the distribution of magnetic flux and bolted to a rectangular steel base. The base consists of two 60 ton castings, the uprights are also 60 tons each, and the total mass of the magnet is about 300 tons. The yoke and coils were bought from industry to CERN specifications. Power consumption was 700 kW.

The magnet was assembled and tested, and the field mapped at ISR point 8 during the 1978–9 winter shutdown (Fig. 4.24), to be used by The Axial Field Spectrometer Collaboration (R807) [26], in conjunction with the superconducting high luminosity insertion [Highlight 4.4] until the ISR was closed in 1983. It was later installed at LEAR as the magnetic spectrometer for the OBELIX experiment. The field-shaping concept was further developed [63], was adopted by the PHENIX collaboration for the "Relativistic Heavy Ion Collider" RHIC at Brookhaven [64], and featured in proposals for experiments at high energy hadron colliders (SSC and LHC) [63, 65].

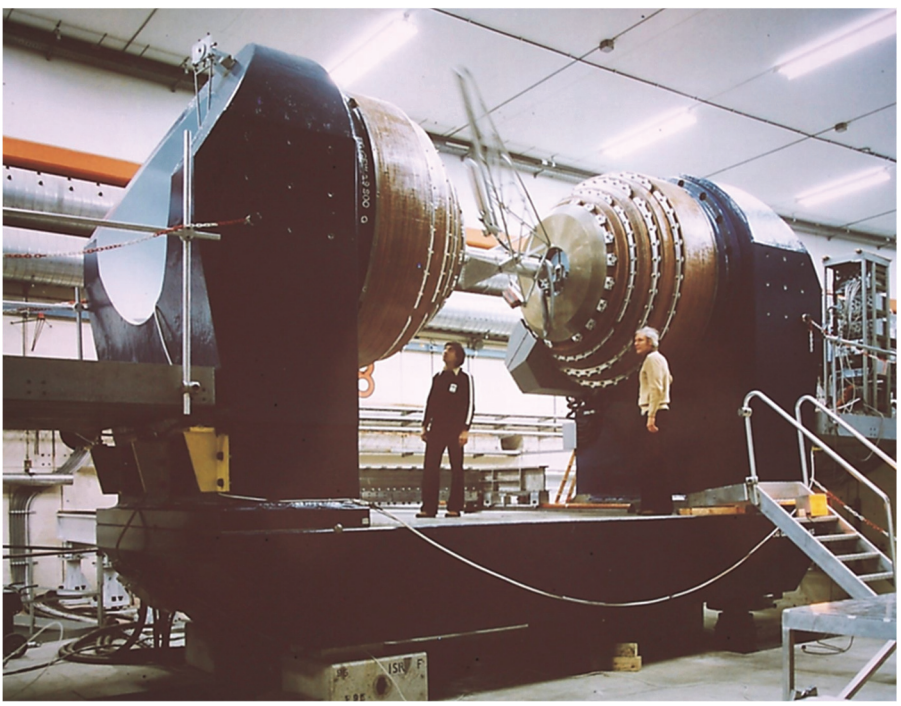

Fig. 4.24. OAFM during the field mapping campaign.

References

1. D. Pestre, The second generation of accelerators for CERN, 1956–1965: the decision process, pp. 679–778 in *History of CERN, Vol. II, Building and running the Laboratory*, by A. Hermann, J. Krige, U. Mersits and D. Pestre (North Holland, 1990).
2. A. Russo, The ISR. The construction and operation of CERN's second large machine and a survey of its experimental programme, pp. 100–170 in *History of CERN, Vol. III*, ed. J. Krige, **(**North Holland, 1996).
3. K. Johnsen, The ISR and accelerator physics, *Particle Accelerators*, **18**, 167-182 (1986).
4. K. Hübner and T. Taylor, The birth and development of the first hadron collider, the ISR, in PAS *Symposium Subnuclear Physics*, 119 (2011).
   https://cds.cern.ch/record/1626809/files/CERN-ACC-2013-0248.pdf;
   P.J. Bryant, p. 15 in *40th Anniversary of the First Proton-Proton Collisions in the CERN Intersecting Storage Rings (ISR)*, U. Amaldi, P.J. Bryant, P. Darriulat and K. Hübner (eds.), CERN 2012- 004 (CERN, Geneva, 2012), http://dx.doi.org/10.5170/CERN-2012-004.15.
5. M. Jacob, *CERN: 25 years of physics* (North-Holland, 1981).
6. U. Amaldi, Small-angle physics at the ISR forty years later, *Report CERN 2012-004* (2012).
7. P. Darriulat, p. 63 in *40th Anniversary of the First Proton-Proton Collisions in the CERN Intersecting Storage Rings (ISR)*, U. Amaldi, P.J. Bryant, P. Darriulat and K. Hübner (eds.), CERN 2012- 004 (CERN, Geneva, 2012), http://dx.doi.org/10.5170/CERN-2012-004.63.
8. Jerome I. Friedman, Henry W. Kendall, Richard E. Taylor, Nobel Prize in Physics 1990; https://www.nobelprize.org/nobel_prizes/physics/laureates/1990.
9. C.W. Fabjan, Evolution and revolution: detectors at the ISR, *CERN COURIER*, January 2011.
10. G. Giacomelli and M. Jacob, Physics at the CERN-ISR, *Phys. Reports* **55**, 1 (1979).
11. C.W. Fabjan and N. McCubbin, Physics at the ISR 1978–1983, *Physics Reports* **403-404**, 165–175 (2004).
12. C. Benvenuti and R.S. Calder, The desorption of condensed hydrogen from various substrates by infrared thermal radiation, *Physics letters* **35A**, No. 4, 291 (1971).
13. C. Benvenuti, Study of a cryopump for possible use in the ISR, *Le Vide* **168**, 235 (1973).
14. C. Benvenuti and M. Firth, Improved version of the CERN condensation cryopump, *Vacuum*, **29**, No. 11/12, 427 (1979).
15. C. Benvenuti and N. Hilleret, Cold bore experiments at CERN ISR, *IEEE trans. Nucl. Sci*. **NS-26**, No. 3, 4086 (1979).
16. D. Alpert (1958), p. 624 in *Encyclopaedia of Physics* **12,** ed. S. Flügge (Springer, Berlin, 1958).
17. C. Benvenuti and M. Hauer, Low pressure limit of the Bayard-Alpert gauge*, Nucl. Instr. & Meth*. **140**, 453 (1977).
18. J.-C. Helmer and W.H. Hayward, Ion gauge for vacuum pressure measurements below 10^{-10} Torr, *Rev. Sci. Instr*. **37**, 1652 (1966).
19. B. Angerth and Z. Hulek, The tungsten evaporation limit of hot-cathode ionization gauges, *J. Vac. Sci. Technol.* **11**, No 1, 481 (1974).
20. C. Benvenuti and M. Hauer, Improved Helmer gauge for measuring pressures down to 10^{-12} Pa, *Le Vide* **201**, (Suppl.) 199 (1980).
21. J. Billan, R. Perin, L. Resegotti, T. Tortschanoff and R. Wolf (eds.) *Construction of a Prototype Superconducting Quadrupole Magnet for a High Luminosity Insertion at the CERN Intersecting Storage Rings*, CERN-1976-016 (CERN, Geneva, 1976).
    http://dx.doi.org/10.5170/CERN-1976-016.

22. L. Resegotti, Superconducting low-beta insertion and high luminosity prospect at ISR, *Report CERN ISR-BOM/77-58* (1977).
23. R. Perin, T. Tortschanoff and R. Wolf, Magnetic design of the superconducting quadrupole magnets for the ISR high luminosity insertion, Report CERN ISR-BOM/79-2 (1979); https://cds.**cern**.ch/record/119973/files/**1979**04141.pdf.
24. R. Perin, Mechanical stability of superconducting quadrupole coils, *Proc. 5th Int. Conf. on Magnet Technology*, Rome (1975) p. 559.
25. J. Billan *et al*., The eight superconducting quadrupoles for the ISR high luminosity insertion, *Proc. XI Int. Conf. on High Energy Accelerators,* CERN, Geneva (1980) p. 848.
26. H. Gordon *et al.*, The Axial Field Spectrometer at the CERN ISR, *Nucl. Instr. & Meth*. **196**, 303–313 (1982).
27. J. Billan *et al*., Operational experience with the superconducting high-luminosity insertion in the CERN Intersecting Storage Ring, *IEEE Trans. Nucl. Sci*. **NS-30**, No. 4 (1983).
28. J. Billan *et al.*, A superconducting high-luminosity insertion in the Intersecting Storage Rings (ISR), *IEEE Trans. Nucl. Sci.* **26**, 3179-3181 (1979).
29. H. Laeger and Ph. Lebrun, The helium cryogenic system for the superconducting high-luminosity insertion at the CERN-ISR, *Adv. Cryo. Eng.* **29**, 359–367 (1984).
30. P. Lebrun, pp. 41-86 in *Proc. of the CERN Accelerator School: Superconductivity in Particle Accelerators*, *DESY*, *Hamburg*, *Germany*, *30 May - 3 Jun 1988*, S. Turner (ed.), CERN-1989-004 (CERN, Geneva, 1989), http://dx.doi.org/10.5170/CERN-1989-004.41.
31. H. Laeger, Ph. Lebrun and P. Rohmig, Eight liquid helium cryostats for the superconducting magnets of the ISR high-luminosity insertion, *Proc. ICEC 8,* Genoa (1980) pp. 124-129.
32. H. Blessing, H. Laeger and Ph. Lebrun, Modular thermostatic vapour-cooled current leads for cryogenic service, *Adv. Cryo. Eng.* **29**, 199–206 (1984).
33. H. Laeger, Ph. Lebrun and P. Rohner, Long flexible transfer lines for gaseous and liquid helium, *Cryogenics* **18**, 659–662 (1978).
34. H. Blessing *et al.*, Four hundred meters of flexible cryogenic helium transfer lines*, Proc. ICEC 8,* Genoa (1980) pp. 261–266.
35. H. Blessing *et al.*, High performance flexible cryogenic helium transfer lines, *Adv. Cryo. Eng.* **27**, 761–768 (1982).
36. H. Blessing *et al.*, Controlled downward transfer of saturated liquid helium across large differences in elevation, *Proc. ICEC 12, Southampton,* (1988) 222–226.
37. J.-P. Dauvergne *et al.*, Helium cryogenics at the LEP experimental areas, *Adv. Cryo. Eng.* **35B**, 901–908 (1990).
38. H. Blessing *et al.*, Very low-loss liquid helium transfer with long flexible lines, *Adv. Cryo. Eng.* **35B**, 909–916 (1990).
39. ALEPH Collaboration, Precision electroweak measurements on the Z Resonance, *Phys. Rep.* **427**, 257 (2006).
40. S. van der Meer, Calibration of the effective beam height in the ISR, *Report CERN/ISR–PO/68–31* (1968).
41. G. Carboni *et al*., Precise measurements of proton-antiproton and proton-proton total cross sections at the CERN Intersection Storage Rings, *Nucl. Phys*. **B 254**, 697 (1985).
42. P. Grafstrom and W. Kozanecki, Luminosity determination in proton colliders, *Prog. Part. Phys.* **81**, 97-148 (2015).
43. H. Burkhardt, Optimisation of LHC beam conditions, *Proc. 35th Int. Conf. on High Energy Physics*, Paris (2010).

44. S. White, Determination of the absolute luminosity at the LHC, CERN-Thesis-2010-0139, (2010).
45. M. Froissart, Asymptotic behavior and subtractions in the Mandelstam representation, *Phys. Rev.* **123**, 1053 (1961).
46. U. Amaldi, Proton interactions at high energy, *Scientific American*, November 1973, http://inspirehep.net/record/214689?ln=en.
47. U. Amaldi, An ISR discovery: The Rise of the Proton-Proton Cross-Section, in *60 years of CERN experiments and discoveries*, eds. L. Di Lella and H. Schopper (World Scientific, 2015).
48. R. Battiston *et al.*, The 'Roman Pot' spectrometer and the vertex detector of experiment UA4 at the CERN SPS collider, *Nucl. Inst. & Meth. A* **238**, 35 (1985).
49. G. Matthiae, in *Scattering; scattering and inverse scattering in pure and applied science*, eds. R. Pike and P. Sabatier (Academic Press, 2002).
50. TOTEM Collaboration, Performance of the TOTEM detectors at the LHC*, Int. J. Mod. Phys.* **A28**, 1330046, (2013).
51. G. Charpak, *et al*., The Use of Multiwire Proportional Counters to Select and Localize Charged Particles, *Nucl. Instr. & Meth.* **62**, 262 (1968).
    G. Charpak and F. Sauli, High-resolution electronic particle detectors, *Ann. Rev. Nucl. Part. Sci.* **34**, 285 (1984).
52. G. Charpak*, et al*., Some features of large multiwire proportional chambers, *Nucl. Instr. & Meth.* **97**, 377 (1971).
53. R. Bouclier, *et al*., Proportional Chambers for a 50 000-wire detector*, Nucl. Instr. & Meth.* **115**, 235, (1974).
54. D. Cockerill, *et al*., Operation of a Drift Chamber Vertex Detector at the ISR, *Nucl. Instr. and Meth*. **176**, 159 (1980).
55. F. Sauli and A. Sharma, Micro-Pattern Gaseous Detectors, *Ann. Rev. Nucl. Part. Sci.* **49,** 341 (1999).
56. F. Sauli, Gas Electron Multiplier (GEM) detectors: Principles of Operation and Applications, *Comprehensive Biomedical Physics* **8**, 367 (2014).
57. C. W. Fabjan and W. Struczinski, Coherent emission of transition radiation on periodic radiators, *Phys. Lett*. **57B**, 483 (1975).
58. B. Dolgoshein, Transition radiation detectors, *Nucl. Instr. & Meth. A* **326**, 434 (1993).
59. A. Andronic and J. P. Wessels, Transition radiation detectors, *Nucl. Instr. & Meth. A* **666**, 130 (2012).
60. W. J. Willis and V. Radeka, Liquid-argon ionization chambers as total-absorption detectors, *Nucl. Instr. & Meth*. **120**, 221 (1974).
61. C.W. Fabjan and F. Gianotti, Calorimetry for particle physics, *Rev. Mod. Phys.* **75**, 3 (2003).
62. T. Akesson *et al.*, Properties of a fine sampling uranium-copper scintillator hadron calorimeter, *Nucl. Instr. & Meth. A* **241**, 17 (1985).
63. E. Dolgosheina, T. Taylor and W.J. Willis, Field shaping by iron for muon measurement at hadron colliders, *Nucl. Instr. & Meth. A* **301**, 451-453 (1991).
64. K. Adox *et al*., PHENIX detector overview, *Nucl. Instr. & Meth*. *A* **499**, 469 (2003).
65. A. Dudragne *et al.*, A shaped solenoid for muon spectroscopy at high energy hadron colliders, *Nucl. Instr. & Meth*. *A* **324**, 93 (1993).